

**Thermoosmosis of a near-critical binary fluid mixture:
a general formulation and universal flow direction**

Youhei Fujitani*

*School of Fundamental Science and Technology,
Keio University, Yokohama 223-8522, Japan*

Shunsuke Yabunaka†

*Advanced Science Research Center,
Japan Atomic Energy Agency, Tokai, 319-1195, Japan*

(Dated: September 21, 2023)

Abstract

We consider a binary fluid mixture, which lies in the one-phase region near the demixing critical point, and study its transport through a capillary tube linking two large reservoirs. We assume that short-range interactions cause preferential adsorption of one component on the tube's wall. The adsorption layer can become much thicker than the molecular size, which enables us to apply hydrodynamics based on a coarse-grained free-energy functional. For linear transport phenomena induced by gradients of the pressure, composition, and temperature along a cylindrical tube, we obtain the formulas of the Onsager coefficients to extend our previous results on isothermal transport, assuming the critical composition in the middle of each reservoir in the reference equilibrium state. Among the linear transport phenomena, we focus on thermoosmosis — mass flow due to a temperature gradient. We explicitly derive a formula for the thermal force density, which is nonvanishing in the adsorption layer and causes thermoosmosis. This formula for a near-critical binary fluid mixture is an extension of the conventional formula for a one-component fluid, expressed in terms of local excess enthalpy. We predict that the direction of thermoosmotic flow of a mixture near the upper (lower) consolute point is the same as (opposite to) that of the temperature gradient, irrespective of which component is adsorbed on the wall. Our procedure would also be applied to dynamics of a soft material, whose mesoscopic inhomogeneity can be described by a coarse-grained free-energy functional.

PACS numbers:

*Electronic address: youhei@appi.keio.ac.jp

†Electronic address: yabunaka123@gmail.com

I. INTRODUCTION

Osmotic transport of a fluid through a channel at micrometer, or smaller scales, has gained much attention because it is applied in lab-on-a-chip processes [1–5] and involves fundamental problems in nonequilibrium physics [6–11]. A gradient of temperature (concentration) along the channel induces a flow, called thermoosmosis (diffusioosmosis), because of force density generated in a heterogeneous layer near the wall [12–14]; thermoosmosis does not involve the buoyancy responsible for thermal convection. Derjaguin and his coworkers rationalize thermoosmosis and diffusioosmosis in terms of the continuum description [15–17].

For a one-component fluid, Derjaguin and Sidorenkov (DS) [15] derived a formula of the thermal force density, which causes thermoosmosis. According to DS’s formula, the direction of the flow is the same as (opposite to) that of the temperature gradient if the excess enthalpy density is negative (positive) near the wall. This is naively expected since the flow in this direction tends to eliminate the temperature gradient by carrying the fluid with lower (higher) enthalpy to the region with higher (lower) temperature. However, there exist several difficulties when applying this formula to experimental systems as follows. Firstly, the thickness of the heterogeneous layer is microscopic and the continuum description cannot incorporate details inside the layer very precisely [6, 11]. Secondly, the local excess enthalpy is not easy to access experimentally. Its evaluation based on microscopic models has been studied [6, 18], whereas well-definedness of its microscopic expression is questioned especially near the surface [6, 19]. In Ref. [6], the authors extend DS’s formula for a multicomponent fluid in the continuum description, while noticing the difficulties discussed above. Therefore, it remains often hard to understand even the flow direction in thermoosmosis [7].

Thermoosmosis has not been studied in relation to critical phenomena to our best knowledge. In the present study, for a binary fluid mixture lying in the one-phase region close to the demixing critical point, we extend our previous study on isothermal dynamics [20] to cover non-isothermal dynamics of thermoosmosis. Below, this mixture, simply referred to as a mixture, is assumed to be filled in a container composed of two large reservoirs and a capillary tube connecting them. The tube’s wall is impermeable and adiabatic. Differences

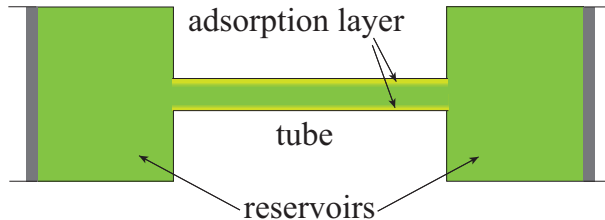


FIG. 1: Schematic of a situation supposed in our formulation. A mixture is filled in the container composed of two reservoirs and a capillary tube connecting them. One component drawn in yellow is preferentially adsorbed by the tube’s wall, which is impermeable and adiabatic. There may be preferential adsorption onto the reservoir’s wall, which is not supposed in this figure. Thick walls represent pistons. Imposing difference in pressure, composition, and/or temperature between the reservoirs generates a mass flow through the tube.

in temperature, composition, and pressure can be imposed between the two reservoirs (Fig. 1). A short-range interaction is assumed between each mixture component and tube’s wall, which in general attracts one component more than the other. The resulting preferential adsorption (PA), becoming remarkable owing to large osmotic susceptibility [21, 22], has been studied for a long time [23–26]. The adsorption layer can be much thicker than the molecular size. Thus, it is expected that we can study transport of a mixture through a tube in terms of the continuum description, avoiding its difficulty mentioned in the last paragraph. In Ref. [20], applying the hydrodynamics based on a coarse-grained free-energy functional [27], the present authors studied isothermal transport in the linear regime with respect to thermodynamic forces to calculate the involved Onsager coefficients and conductance in diffusioosmosis.

Order-parameter fluctuations in a mixture, being significant on length scales smaller than the correlation length, enhance the transport coefficients to cause universal properties [28–32]. However, the PA keeps the mixture composition in a tube away from the critical one, in particular near the tube’s wall, and thus the critical enhancement does not affect diffusioosmosis of a mixture significantly [20]. Hydrodynamics can be applied to a flow in the tube, where the correlation length is locally smaller than a typical length of the flow. It is also suggested in Ref. [20] that, in a critical regime, the mixture velocity due to diffusioosmosis far from a flat surface should exhibit a power-law dependence on the

difference between the mixture temperature and the critical temperature if the adsorption is sufficiently strong. This originates from the universal order-parameter profile at equilibrium [33, 34]. The same power law is numerically suggested for the diffusiophoretic mobility of a colloidal particle in a mixture [35, 36].

In the present study, we extend our previous procedure of Ref. [20] to cover non-isothermal dynamics. Our general formulation is described in Sections II A and II B. We employ the hydrodynamics under inhomogeneous temperature formulated from a coarse-grained free-energy functional [37, 38]. Imposing the no-slip condition at the tube's wall and neglecting effects of the tube's edges, we discuss flow fields in the tube in the linear regime in Section II C. In Sections III A and III B, we derive formulas for the Onsager coefficients and a formula of the thermal force density for a cylindrical tube, assuming the total mass density to be homogeneous inside the tube and the mixture composition to be critical in the middle of a reservoir in the reference equilibrium state. The former formulas include extensions of our previous results of Ref. [20] to non-isothermal transport, whereas the latter can be regarded as an extension of DS's formula to a mixture considered here. We apply the renormalized local functional theory [33, 39] to specify the free-energy functional in Section III C, and rewrite our formulas in Section III D. This theory can incorporate the effects of the critical fluctuations when the correlation length is spatially varying as is the case in the adsorption layer. In Section IV, we focus on thermoosmosis to show numerical results, and predict that, irrespective of which component is adsorbed on the wall, the flow direction is the same as (opposite to) the direction of the temperature gradient in thermoosmosis of a mixture near the upper (lower) consolute point. Further discussion and summary are given in Section V. Some of our results are also discussed in the companion Letter [40].

II. FORMULATION

We write ρ_a (ρ_b) for the mass density of a mixture component named a (b). The sum $\rho_a + \rho_b$ is denoted by ρ , which represents the total mass density, whereas the difference $\rho_a - \rho_b$ is denoted by φ . We write c_n for the mass fraction ρ_n/ρ and μ_n for the chemical potential conjugate to ρ_n , where n is a or b. In an equilibrium mixture with homogeneous mass densities, μ_n is a function of the temperature (denoted by T), pressure (P), and c_a ,

and is also a function of T , ρ , and φ . We write μ_{\pm} for $(\mu_a \pm \mu_b)/2$; ρ and φ are conjugate to μ_+ and μ_- , respectively. Difference of a quantity in the left reservoir subtracted from the quantity in the right is indicated by δ . For example, $\delta\mu_a$ denotes the difference in μ_a between the reservoirs. If the reservoir's wall adsorbs a component more, φ can be inhomogeneous near the wall. For such a quantity, δ indicates the difference between the central regions of the reservoirs. The difference between the pressures on the pistons is given by δP .

A. Thermodynamics

We first consider entropy fluctuations of an equilibrium mixture in the isolated container with the pistons fixed (Fig. 1). The total mass of the component n in the right reservoir is denoted by \mathcal{M}_{nR} . Neglecting the contribution from the mixture in the tube, we can regard the total entropy of the mixture in the container, denoted by S , as a function of \mathcal{M}_{aR} , \mathcal{M}_{bR} , and the internal energy of the mixture in the right reservoir, \mathcal{U}_R . With t denoting the time,

$$\frac{dS}{dt} = \frac{d\mathcal{U}_R}{dt} \delta \left(\frac{1}{T} \right) + \frac{d\mathcal{M}_{nR}}{dt} \delta \left(\frac{-\mu_n}{T} \right) \quad (1)$$

holds up to the second order of the magnitudes of the deviations. Repeated indices are summed hereafter. Equation (1) is included in Eq. (XV-55) of Ref. [41]. The thermodynamic fluxes are given by the time derivatives on the right-hand side (RHS) and are driven by the conjugate thermodynamic forces, $\delta(1/T)$ and $-\delta(\mu_n/T)$. They are respectively the partial derivatives of S with respect to \mathcal{U}_R and \mathcal{M}_{nR} [42].

We assume that weak thermodynamic forces are imposed on an equilibrium mixture. This equilibrium state is close to the critical point and is referred to as reference state. We add a superscript ^(ref) to a quantity in the middle of a reservoir in the reference state. For example, $\rho_n^{(\text{ref})}$ denotes ρ_n in the central regions in the reference state. Writing u for the internal energy per unit volume, we apply the Gibbs-Duhem (GD) relation to obtain

$$\begin{pmatrix} -\delta(P/T) \\ -\delta(\mu_-/T) \\ \delta(1/T) \end{pmatrix} = \begin{pmatrix} \rho_a^{(\text{ref})} & \rho_b^{(\text{ref})} & u^{(\text{ref})} \\ 1/2 & -1/2 & 0 \\ 0 & 0 & 1 \end{pmatrix} \begin{pmatrix} -\delta(\mu_a/T) \\ -\delta(\mu_b/T) \\ \delta(1/T) \end{pmatrix}, \quad (2)$$

whose left-hand side (LHS) gives a new set of thermodynamic forces. We write Θ for the coefficient matrix on the RHS above. The thermodynamic fluxes conjugate to the respective

components of the new set, denoted by \mathcal{I} , \mathcal{J} , and \mathcal{K} , are defined by the first equality of

$$(\Theta^{-1})^T \begin{pmatrix} d\mathcal{M}_{\text{aR}}/(dt) \\ d\mathcal{M}_{\text{bR}}/(dt) \\ d\mathcal{U}_{\text{R}}/(dt) \end{pmatrix} = \begin{pmatrix} \mathcal{I} \\ \mathcal{J} \\ \mathcal{K} \end{pmatrix} = L \begin{pmatrix} -\delta(P/T) \\ -\delta(\mu_-/T) \\ \delta(1/T) \end{pmatrix}, \quad (3)$$

where the superscript T indicates the transposition. The second equality above represents linear phenomenological equations; a matrix L is here introduced and their components are Onsager coefficients considered later.

The partial volume and partial entropy per unit mass of the component n , are denoted by \bar{v}_n and \bar{s}_n , respectively. In an equilibrium mixture with homogeneous densities, we have

$$\bar{v}_n = \left. \frac{\partial \mu_n}{\partial P} \right)_{T, c_a} \quad \text{and} \quad \bar{s}_n = - \left. \frac{\partial \mu_n}{\partial T} \right)_{P, c_a}, \quad (4)$$

where the subscript of a right parenthesis indicates the fixed variables in the partial differentiation. Writing s for the entropy per unit volume, we have

$$1 = \bar{v}_a \rho_a + \bar{v}_b \rho_b \quad \text{and} \quad s = \bar{s}_a \rho_a + \bar{s}_b \rho_b \quad (5)$$

at equilibrium with ρ_n and s being homogeneous. Writing \bar{v}_- and \bar{s}_- for $(\bar{v}_a - \bar{v}_b)/2$ and $(\bar{s}_a - \bar{s}_b)/2$, respectively, we obtain

$$\delta \mu_- = -\bar{s}_-^{(\text{ref})} \delta T + \bar{v}_-^{(\text{ref})} \delta P + \left. \frac{\partial \mu_-}{\partial c_a} \right)_{T, P} \delta c_a, \quad (6)$$

where the partial derivative is evaluated in the middle of a reservoir in the reference state. Thus, the thermodynamic forces in Eq. (3) are determined by δT , δP , and δc_a , and determine $\delta \mu_+$ because the GD relation gives

$$\delta P = \rho_n^{(\text{ref})} \delta \mu_n + s^{(\text{ref})} \delta T = \rho^{(\text{ref})} \delta \mu_+ + \varphi^{(\text{ref})} \delta \mu_- + s^{(\text{ref})} \delta T. \quad (7)$$

B. Hydrodynamics

We consider the Helmholtz free-energy of a mixture as a functional of fields coarse-grained up to the local correlation length of the order-parameter fluctuations. The length is denoted by ξ . A part of the functional is given by the volume integral of a function over the mixture region, V_{tot} . The function, denoted by f_{bulk} , is assumed to depend on ρ_a , ρ_b , their gradients,

and T , with the dependence on the gradients being via $|\nabla\rho_a|^2$, $|\nabla\rho_b|^2$ and $(\nabla\rho_a) \cdot (\nabla\rho_b)$. The other part, representing the wall-component interaction, is assumed to be given by the area integral of a function over the interface, ∂V_{tot} . This function is denoted by f_{surf} and depends on ρ_a , ρ_b , and T . Thus, the free-energy functional is given by

$$F[T, \rho_a, \rho_b] = \int_{V_{\text{tot}}} d\mathbf{r} f_{\text{bulk}}(T, \rho_a, \rho_b, \nabla\rho_a, \nabla\rho_b) + \int_{\partial V_{\text{tot}}} dA f_{\text{surf}}(T, \rho_a, \rho_b) , \quad (8)$$

where T and ρ_n depend on the position \mathbf{r} . The volume element and the area element are represented by $d\mathbf{r}$ and dA , respectively.

We can formulate hydrodynamics on length scales larger than ξ by using Eq. (8). If T is homogeneous, $\mu_n(\mathbf{r})$ is given by the functional derivative of the first term on the RHS of Eq. (8) with respect to $\rho_n(\mathbf{r})$ in V_{tot} . Otherwise, it is given by

$$\mu_n = \frac{\partial f_{\text{bulk}}}{\partial \rho_n} - T \nabla \cdot \left[\frac{1}{T} \frac{\partial f_{\text{bulk}}}{\partial (\nabla \rho_n)} \right] . \quad (9)$$

The reversible part of the pressure tensor, denoted by Π , is given by

$$\Pi = P\mathbf{1} + (\nabla\rho_n) \frac{\partial f_{\text{bulk}}}{\partial (\nabla\rho_n)} , \quad (10)$$

which is symmetric. Here, $\mathbf{1}$ is the identity tensor of order two. The scalar pressure P is given by the negative of the grand-potential density,

$$P = \mu_n \rho_n - f_{\text{bulk}} = \mu_{+\rho} + \mu_{-\varphi} - f_{\text{bulk}} . \quad (11)$$

Equations (9) and (10) are derived for a one-component fluid in Ref. [37] and are applied in a straightforward way to a binary fluid mixture [38]. The previous derivation is not applicable to the free-energy density introduced in Section III C because the coefficient of its square-gradient term, $M_-/2$ in f_{bulk} of Eq. (48), depends on T slightly nonlinearly. The linear dependence is assumed in the previous derivation. In Appendix A, we show a more general derivation, which is applicable to f_{bulk} of Eq. (48). Strictly speaking, this derivation remains relevant to our later calculation of thermoosmosis under the linear regime, because the hydrodynamic equations including this nonlinearity must be derived before their linearization with respect to the temperature gradient. Equations (9) and (10) yield an extended GD formula

$$\nabla \cdot \Pi = \nabla \cdot \Pi^T = \rho_n \nabla \mu_n + s \nabla T + \frac{\nabla T}{T} \cdot \frac{\partial f_{\text{bulk}}}{\partial (\nabla \rho_n)} \nabla \rho_n , \quad (12)$$

which is consistent with principles of linear nonequilibrium thermodynamics; Eq. (12) guarantees positive entropy production rate after combined with irreversible terms and the Onsager's reciprocity for osmotic fluxes through the tube. The former is shown in Ref. [37], whereas the latter is mentioned below Eq. (32) in the next subsection.

The velocity field, \mathbf{v} , is defined in the frame fixed to the container. The time-derivative of ρ equals $-\nabla \cdot (\rho\mathbf{v})$. In the stationary state, we have

$$0 = \nabla \cdot (\rho\mathbf{v}) . \quad (13)$$

Because of the mass conservation of each component, the time derivative of ρ_n is equal to the negative of the divergence of its flux, whose deviation from the convective part, $\rho_n\mathbf{v}$, gives the diffusion flux, denoted by \mathbf{j}_n . It is defined so that $\mathbf{j}_a + \mathbf{j}_b$ vanishes. In the stationary state, we have

$$0 = \nabla \cdot (\varphi\mathbf{v} + \mathbf{j}) , \quad (14)$$

where \mathbf{j} is defined as $\mathbf{j}_a - \mathbf{j}_b$.

Assuming that δT , δP , and δc_a are proportional to a dimensionless smallness parameter, ε , we consider the dynamics in the tube at the order of ε in Section II C. The superscripts (0) and (1) are used to indicate the order of ε . For example, we have $\mu_{\pm} = \mu_{\pm}^{(0)} + \varepsilon\mu_{\pm}^{(1)}$ up to the order of ε , $\mu_{\pm}^{(0)} = \mu_{\pm}^{(\text{ref})}$, and $T^{(0)} = T^{(\text{ref})}$. In contrast, $\rho_n^{(0)}$ becomes inhomogeneous and different from $\rho_n^{(\text{ref})}$ in the presence of PA. Because the fields are assumed to be coarse-grained up to ξ , the mass densities at the equilibrium specified by $T^{(\text{ref})}$ and $\mu_n^{(\text{ref})}$ minimize the grand-potential functional,

$$F[T^{(\text{ref})}, \rho_a, \rho_b] - \int_{V_{\text{tot}}} d\mathbf{r} \left[\mu_+^{(\text{ref})} \rho(\mathbf{r}) + \mu_-^{(\text{ref})} \varphi(\mathbf{r}) \right] . \quad (15)$$

Thus, $\rho_n^{(0)}$ is the solution of Eq. (9) with T and μ_n being replaced by $T^{(\text{ref})}$ and $\mu_n^{(\text{ref})}$, respectively, together with the boundary conditions given by Eq. (A8).

C. Fields in the tube

In this subsection, we consider stationary and laminar flow in the tube at the order of ε . The mixture is assumed to remain in one-phase region throughout inside the container. As

in the previous study [20], we assume that the tube is so long and thin that effects of the tube's edges on the flow are negligible. We regard $\delta\mu_n$ and δT as equal to the differences in μ_n and T between the edges, respectively; μ_n and T are assumed to be homogeneous over the tube's cross-section at each edge.

Assuming the tube to extend along the z axis with the same cross-section, we take the Cartesian coordinates (x, y, z) with the right reservoir lying on the positive z side. A field with the superscript (0) , such as $\rho_n^{(0)}$, is independent of z in the tube. We apply Eq. (13) for a laminar flow to obtain

$$0 = \nabla \cdot \mathbf{v}^{(1)} = \partial_z v_z^{(1)} , \quad (16)$$

without assuming the mixture to be incompressible. Here, ∂_z denotes the partial derivative with respect to z . In the tube up to the order of ε , the momentum conservation gives

$$2\nabla \cdot (\eta_s \mathbf{E}) = \nabla \cdot \Pi , \quad (17)$$

where η_s is the shear viscosity and \mathbf{E} is the rate-of-strain tensor. Owing to the critical enhancement, η_s depends on the local correlation length, ξ . Writing $\eta_s^{(0)}$ for η_s evaluated at $\varepsilon = 0$, we rewrite the LHS of Eq. (17) as ε multiplied by

$$2\nabla \cdot (\eta_s^{(0)} \mathbf{E}^{(1)}) = \nabla \cdot \left\{ \eta_s^{(0)} \left[\nabla \mathbf{v}^{(1)} + (\nabla \mathbf{v}^{(1)})^T \right] \right\} . \quad (18)$$

With the aid of Eq. (12), we rewrite the RHS of Eq. (17) as ε multiplied by

$$\nabla \cdot \Pi^{(1)} = \rho_n^{(0)} \nabla \mu_n^{(1)} + s^{(0)} \nabla T^{(1)} + \frac{\nabla T^{(1)}}{T^{(0)}} \cdot \frac{\partial f_{\text{bulk}}}{\partial (\nabla \rho_n)} (\nabla \rho_n^{(0)}) , \quad (19)$$

where the partial derivative of f_{bulk} is evaluated at $\varepsilon = 0$. In the absence of PA, $\rho_n^{(0)}$ and $\eta_s^{(0)}$ are homogeneous, and thus Eq. (17) becomes the usual Stokes equation, $\eta_s \Delta \mathbf{v} = \nabla P$, owing to Eq. (10).

Writing u (e) for the internal (total) energy per unit volume, we have $u = e - \rho |\mathbf{v}|^2 / 2$,

$$s = - \left. \frac{\partial f_{\text{bulk}}}{\partial T} \right)_{\rho_n, \nabla \rho_n} , \text{ and } u = f_{\text{bulk}} + Ts = -T^2 \left. \frac{\partial}{\partial T} \frac{f_{\text{bulk}}}{T} \right)_{\rho_n, \nabla \rho_n} \quad (20)$$

in V_{tot} . The heat flux, denoted by \mathbf{j}_q , is defined so that the Eulerian time-derivative of e equals $-\nabla \cdot (e\mathbf{v} + \mathbf{v} \cdot \Pi + \mathbf{j}_q)$. In a stationary state in the tube, we have

$$0 = \nabla \cdot \left(u^{(0)} \mathbf{v}^{(1)} + \mathbf{v}^{(1)} \cdot \Pi^{(0)} + \mathbf{j}_q^{(1)} \right) , \quad (21)$$

where $u^{(0)}$ equals $e^{(0)}$. We can define the transport coefficients, Λ , λ , and κ , so that

$$\mathbf{j} = -T\Lambda\nabla\frac{\mu_-}{T} + \kappa\nabla\frac{1}{T} \quad \text{and} \quad \mathbf{j}_q = -\kappa\nabla\frac{\mu_-}{T} + \lambda\nabla\frac{1}{T} \quad (22)$$

hold [41, 42]. The coefficients depend on ξ owing to the critical enhancement. If evaluated using ξ at $\varepsilon = 0$, they are denoted by $\Lambda^{(0)}$, $\kappa^{(0)}$, and $\lambda^{(0)}$, respectively, and are independent of z . In Eq. (22) at the order of ε , we can use $T^{(0)}\Lambda^{(0)}$, $\kappa^{(0)}$, and $\lambda^{(0)}$ for $T\Lambda$, κ , and λ , respectively.

With the aid of Eqs. (18) and (19), the x and y components of Eq. (17) give

$$0 = \rho^{(0)}\bar{\nabla}\mu_+^{(1)} + \varphi^{(0)}\bar{\nabla}\mu_-^{(1)} + s^{(0)}\bar{\nabla}T^{(1)} , \quad (23)$$

where $\bar{\nabla}$ represents the two-dimensional nabla defined on the (x, y) plane. Because $P^{(0)}$, $\rho_n^{(0)}$, and $u^{(0)}$ are independent of z , we obtain

$$\nabla \cdot \mathbf{j}^{(1)} = 0 \quad \text{and} \quad \nabla \cdot \mathbf{j}_q^{(1)} = 0 . \quad (24)$$

The first entry comes from Eqs. (14) and (16), whereas the second from Eqs. (10), (12), and (21). The components of \mathbf{j} and \mathbf{j}_q normal to the tube's wall vanish at the impermeable and adiabatic wall. These conditions, the conditions at the tube's edges mentioned in the beginning of Section II C, Eq. (23), and Eq. (24) are satisfied if $\mu_n^{(1)}$ and $T^{(1)}$ are linear functions of z and are independent of x and y . Then, $\mathbf{j}^{(1)}$ and $\mathbf{j}_q^{(1)}$ have only z components and are independent of z , considering Eq. (22) up to the order of ε . With the aid of Eqs. (18) and (19), the z component of Eq. (17) give

$$\bar{\nabla} \cdot (\eta_s^{(0)}\bar{\nabla}v_z^{(1)}) = \rho_n^{(0)}\partial_z\mu_n^{(1)} + s^{(0)}\partial_zT^{(1)} , \quad (25)$$

where $v_z^{(1)}$ is regarded as a scalar on a cross-section. The derivatives on the RHS above are constants determined by the thermodynamic forces in Eq. (3). Writing L_{tube} for the tube length, we obtain

$$\varepsilon\partial_zT^{(1)} = -\frac{T^{(0)2}}{L_{\text{tube}}}\delta\left(\frac{1}{T}\right) , \quad \varepsilon\partial_z\mu_-^{(1)} = \frac{T^{(0)}}{L_{\text{tube}}}\left[\delta\left(\frac{\mu_-}{T}\right) - \mu_-^{(0)}\delta\left(\frac{1}{T}\right)\right] , \quad (26)$$

and

$$\varepsilon\partial_z\mu_+^{(1)} = \frac{1}{\rho^{(\text{ref})}L_{\text{tube}}}(\delta P - \varphi^{(\text{ref})}\delta\mu_- - s^{(\text{ref})}\delta T) , \quad (27)$$

with the aid of Eq. (7). Thus, we use Eqs. (11) and (20) to rewrite Eq. (25) as

$$\begin{aligned} \varepsilon \bar{\nabla} \cdot (\eta_s^{(0)} \bar{\nabla} v_z^{(1)}) &= \frac{T^{(0)}}{L_{\text{tube}}} \left\{ \frac{\rho^{(0)}}{\rho^{(\text{ref})}} \delta \left(\frac{P}{T} \right) + \left(\varphi^{(0)} - \frac{\rho^{(0)} \varphi^{(\text{ref})}}{\rho^{(\text{ref})}} \right) \delta \left(\frac{\mu_-}{T} \right) \right. \\ &\quad \left. + \left(\frac{\rho^{(0)} u^{(\text{ref})}}{\rho^{(\text{ref})}} - u^{(0)} - P^{(0)} \right) \delta \left(\frac{1}{T} \right) \right\}. \end{aligned} \quad (28)$$

This determines $v_z^{(1)}$, which is independent of z because of Eq. (16), together with the boundary conditions. From Eq. (22), we obtain

$$\varepsilon j_z^{(1)} = \frac{1}{L_{\text{tube}}} \left[T^{(0)} \Lambda^{(0)} \delta \left(\frac{-\mu_-}{T} \right) + \kappa^{(0)} \delta \left(\frac{1}{T} \right) \right] \quad (29)$$

and

$$\varepsilon j_{qz}^{(1)} = \frac{1}{L_{\text{tube}}} \left[\kappa^{(0)} \delta \left(\frac{-\mu_-}{T} \right) + \lambda^{(0)} \delta \left(\frac{1}{T} \right) \right] \quad (30)$$

in the tube. Up to the order of ε , $d\mathcal{M}_{nR}/(dt)$ and $d\mathcal{U}_R/(dt)$ are respectively given by the area integral of $\varepsilon(\rho_n^{(0)} v_z^{(1)} + j_{nz}^{(1)})$ and that of $\varepsilon(u^{(0)} + P^{(0)})v_z^{(1)} + \varepsilon j_{qz}^{(1)}$ over a tube's cross-section, which is denoted by S_{tube} . Thus, we use the first equality of Eq. (3) to obtain

$$\mathcal{I} = \frac{\varepsilon}{\rho^{(\text{ref})}} \int_{S_{\text{tube}}} dA \rho^{(0)} v_z^{(1)}, \quad \mathcal{J} = \varepsilon \int_{S_{\text{tube}}} dA \left[\left(\varphi^{(0)} - \frac{\rho^{(0)} \varphi^{(\text{ref})}}{\rho^{(\text{ref})}} \right) v_z^{(1)} + j_z^{(1)} \right], \quad (31)$$

and

$$\mathcal{K} = \varepsilon \int_{S_{\text{tube}}} dA \left[\left(u^{(0)} + P^{(0)} - \frac{\rho^{(0)} u^{(\text{ref})}}{\rho^{(\text{ref})}} \right) v_z^{(1)} + j_{qz}^{(1)} \right]. \quad (32)$$

In Appendix B, our formulation up to here is shown to be consistent with Onsager's reciprocal relation, as it should be. Because of Eq. (11), $P^{(0)}$ can be inhomogeneous on a tube's cross-section in the presence of PA. In its absence, because $P^{(0)}$ is homogeneously equal to $P^{(\text{ref})}$, the RHS of Eq. (28), and thus $v_z^{(1)}$, vanish when δP vanishes. This is consistent with the results in Chapter XV-5 of Ref. [41].

With the subscript c , we refer to the value at the critical point determined under the pressure $P^{(\text{ref})}$. The deviation of φ from its value at the critical point, $\varphi - \varphi_c$, plays a role of the order parameter of phase separation and is denoted by ψ . At equilibrium, correlated clusters of ψ are randomly convected on length scales smaller than ξ . On larger length scales, the convection is averaged out to enhance the transport coefficient for the interdiffusion in a mixture at the critical composition, as mentioned in Section I. The critical enhancement suppresses the critical slowing down of the relaxation of the two-time correlation function

of ψ . This function follows the diffusion equation. According to the mode-coupling theory [28], the singular part of the diffusion coefficient coincides with the self-diffusion coefficient of a rigid sphere with the radius being equal to ξ . This result is slightly modified by the dynamic renormalization-group calculation for the model H, with the weak singularity of η_s taken into account [29, 30, 32, 43, 44]. Because multiplying the diffusion coefficient by the osmotic susceptibility, denoted by χ , gives the transport coefficient Λ , we have

$$\Lambda = \frac{\chi R k_B T_c}{\xi \eta_{\text{sing}}}, \quad (33)$$

where R is a universal constant close to $1/(6\pi)$, k_B is the Boltzmann constant, T_c is the critical temperature, and η_{sing} represents the singular part of η_s . The regular part of Λ is usually negligible in the critical regime, judging from the data in Ref. [45] for example. The partial enthalpy per unit mass of the component n , denoted by \bar{H}_n , is given by

$$\bar{H}_n = \mu_n + T \bar{s}_n = -T^2 \left. \frac{\partial}{\partial T} \frac{\mu_n}{T} \right)_{P, c_a} \quad (34)$$

and \bar{H}_- is defined as $(\bar{H}_a - \bar{H}_b)/2$. Neglecting the regular parts in the results of Ref. [46], we use

$$\kappa = \Lambda T \bar{H}_- \quad \text{and} \quad \lambda = \Lambda T (\bar{H}_-)^2. \quad (35)$$

Here, as shown in Appendix C, the second entry contains more approximations, which affect only the formula for L_{33} in the following, than the first entry.

Equation (33) holds at equilibrium with the critical composition. In our problem, to evaluate $\Lambda^{(0)}$, we simply extend this result to a homogeneous off-critical composition and use the extended result even when the composition is inhomogeneous. Hence, we evaluate the RHS of Eq. (33) by using $T^{(0)}$, $\psi^{(0)}(\mathbf{r})$, and the resulting local value of ξ , to obtain $\Lambda^{(0)}$. This is the same procedure as used in Refs. [20, 27]. Likewise, we obtain $\kappa^{(0)}$ and $\lambda^{(0)}$ in the dynamics by replacing Λ , T , and \bar{H}_- with $\Lambda^{(0)}$, $T^{(0)}$, and $\bar{H}_-^{(0)}$, respectively, in Eq. (35).

III. CALCULATION UNDER SOME SPECIFICATIONS

We specify the problem by making the following assumptions. First, we assume f_{surf} to be independent of ρ . Thus, $\rho^{(0)}$ equals $\rho^{(\text{ref})}$ homogeneously. Second, we assume $\psi^{(\text{ref})} = 0$. Third, we assume the tube to be a cylinder with the radius of r_{tube} . In the tube,

a field depends only on the distance from the central axis, r , on a cross-section, and we can write $\psi^{(0)}(r)$, $\eta_s^{(0)}(r)$, $v_z^{(1)}(r)$, and $j_z^{(1)}(r)$, for example. The LHS of Eq. (28) becomes $\varepsilon r^{-1} \partial_r \left(r \eta_s^{(0)} \partial_r v_z^{(1)} \right)$; $v_z^{(1)}$ vanishes at $r = r_{\text{tube}}$ owing to the no-slip condition and $\partial_r v_z^{(1)}$ vanishes at $r = 0$ owing to the axisymmetry and smoothness of $v_z^{(1)}$. Thus, in the tube, we obtain

$$\varepsilon v_z^{(1)}(r) = \int_r^{r_{\text{tube}}} dr_1 \frac{1}{r_1 \eta_s^{(0)}(r_1)} \int_0^{r_1} dr_2 r_2 \frac{T^{(0)}}{L_{\text{tube}}} \left[\delta \left(\frac{-P}{T} \right) + \psi^{(0)}(r_2) \delta \left(\frac{-\mu_-}{T} \right) + (u^{(0)}(r_2) - u^{(\text{ref})} + P^{(0)}(r_2)) \delta \left(\frac{1}{T} \right) \right] \quad (36)$$

for general thermodynamic forces. Substituting Eqs. (29), (30), and (36) into Eqs. (31) and (32) yields formulas for the components of L in Eq. (3), as shown in Section III A.

A. Formulas for the Onsager coefficients

A dimensionless radial distance \hat{r} is defined as r/r_{tube} . We define T_* so that ξ becomes r_{tube} for $\psi = 0$ at $T = T_*$. A characteristic order parameter ψ_* is defined so that ξ becomes r_{tube} for $\psi = \psi_*$ at $T = T_c$. A dimensionless order-parameter at $\varepsilon = 0$, $\hat{\psi}^{(0)}(\hat{r})$, is defined as $\psi^{(0)}(\hat{r} r_{\text{tube}})/\psi_*$. A characteristic chemical potential, μ_* , is defined as

$$\mu_* = \frac{k_B T_*}{3u^* r_{\text{tube}}^3 \psi_*}, \quad (37)$$

where u^* is the scaled coupling constant at the Wilson-Fisher fixed point and equals $2\pi^2/9$ at the one loop order. We define η_* and Λ_* as η_{sing} and Λ at $\psi = 0$ and $T = T_*$, respectively. Dimensionless transport coefficients $\hat{\eta}(\hat{r})$ and $\hat{\Lambda}(\hat{r})$ are defined as $\eta_s^{(0)}/\eta_*$ and $T^{(0)}\Lambda^{(0)}/(T_*\Lambda_*)$ evaluated at $r = \hat{r} r_{\text{tube}}$, respectively. The flow rate of Hagen-Poiseuille flow of a fluid, with the viscosity being η_* , driven by the pressure gradient $\mu_*\psi_*/L_{\text{tube}}$, is denoted by \mathcal{I}_* and is given by

$$\mathcal{I}_* = \frac{\pi r_{\text{tube}}^4 \mu_* \psi_*}{8\eta_* L_{\text{tube}}}. \quad (38)$$

We define a functional $\Omega[g_1, g_2]$, where g_1 and g_2 are functions, as

$$\Omega[g_1, g_2] = 16 \int_0^1 dq_1 q_1 g_1(q_1) \int_{q_1}^1 dq_2 \frac{1}{q_2 \hat{\eta}(q_2)} \int_0^{q_2} dq_3 q_3 g_2(q_3), \quad (39)$$

which is found to be equal to $\Omega[g_2, g_1]$ by exchanging the order of integrals. We have

$$L_{11} = \frac{\mathcal{I}_* T^{(0)}}{\mu_* \psi_*} \Omega[1, 1], \quad L_{12} = L_{21} = \frac{\mathcal{I}_* T^{(0)}}{\mu_*} \Omega[1, \hat{\psi}^{(0)}], \quad (40)$$

and

$$L_{22} = \frac{\mathcal{I}_* \psi_* T^{(0)}}{\mu_*} \Omega[\hat{\psi}^{(0)}, \hat{\psi}^{(0)}] + 2\pi r_{\text{tube}}^2 \frac{\Lambda_* T_*}{L_{\text{tube}}} \int_0^1 d\hat{r} \hat{r} \hat{\Lambda}(\hat{r}). \quad (41)$$

These three formulas are essentially the same as obtained in Ref. [20], where the diffusioosmotic conductance is calculated using L_{12} . Introducing

$$\hat{Y}^{(0)}(\hat{r}) = \frac{1}{\mu_* \psi_*} [u^{(0)} - u^{(\text{ref})} + P^{(0)}] \quad \text{and} \quad \hat{H}_-^{(0)}(\hat{r}) = \frac{\bar{H}_-^{(0)}}{\mu_*}, \quad (42)$$

where $u^{(0)}$, $P^{(0)}$, and $\bar{H}_-^{(0)}$ are evaluated at $r = \hat{r} r_{\text{tube}}$, we obtain new formulas,

$$L_{13} = L_{31} = \mathcal{I}_* T^{(0)} \Omega[1, \hat{Y}^{(0)}], \quad (43)$$

$$L_{23} = L_{32} = \mathcal{I}_* \psi_* T^{(0)} \Omega[\hat{\psi}^{(0)}, \hat{Y}^{(0)}] + 2\pi r_{\text{tube}}^2 \frac{\mu_* \Lambda_* T_*}{L_{\text{tube}}} \int_0^1 d\hat{r} \hat{r} \hat{\Lambda}(\hat{r}) \hat{H}_-^{(0)}(\hat{r}), \quad (44)$$

and

$$L_{33} = \mathcal{I}_* \mu_* \psi_* T^{(0)} \Omega[\hat{Y}^{(0)}, \hat{Y}^{(0)}] + 2\pi r_{\text{tube}}^2 \frac{\mu_*^2 \Lambda_* T_*}{L_{\text{tube}}} \int_0^1 d\hat{r} \hat{r} \hat{\Lambda}(\hat{r}) \left[\hat{H}_-^{(0)}(\hat{r}) \right]^2. \quad (45)$$

The second term on the RHS of Eq. (45) is affected by the approximations mentioned below Eq. (35).

B. Formulas for thermoosmosis

The thermal force density occurs under a temperature gradient and causes thermoosmosis. We write $\sigma_z^{(\text{th})}$ for this density on a tube's cross-section in the linear regime. It is given by the negative of the RHS of Eq. (28), or the z component of $-\varepsilon \nabla \cdot \Pi^{(1)}$, under $\delta T \neq 0$ and $\delta P = \delta c_a = 0$. We have

$$\sigma_z^{(\text{th})}(r) = -\frac{\delta T}{T^{(0)} L_{\text{tube}}} \left(u^{(0)}(r) + P^{(0)}(r) - u^{(\text{ref})} - P^{(\text{ref})} - \bar{H}_-^{(\text{ref})} \psi^{(0)} \right). \quad (46)$$

The factor $\bar{H}_-^{(\text{ref})}$ above comes from $\delta(\mu_-/T)$ via Eqs. (6) and (34). The first four terms in the parentheses above can be interpreted as the excess enthalpy density in DS's formula for a one-component fluid. In the presence of PA, $\Pi_{zz}^{(0)} = P^{(0)}$ is equal to neither $\Pi_{xx}^{(0)}$ nor $\Pi_{yy}^{(0)}$. The occurrence of $\Pi_{zz}^{(0)} = P^{(0)}$ in Eq. (46) is consistent with many author's claim that the

zz component should be involved in the thermal force density near the wall [6, 14].

Here, we compare our derivation of the thermal force density with the corresponding part in Ref. [6], which is mentioned in Section I. Because the sum of the last three terms of Eq. (46) equals $-\rho_a \bar{H}_a^{(\text{ref})} - \rho_b \bar{H}_b^{(\text{ref})}$, thus the negative of Eq. (46), *i.e.*, the formula for $-\sigma_z^{(\text{th})}$, formally coincides with the RHS of Eq. (5) of Ref. [6], where the RHS is treated as the negative of the thermal force density. However, its LHS, $\partial_z \Pi_{zz}$ in our notation, is not equal to $-\sigma_z^{(\text{th})}$ in general, since $\partial_x \Pi_{xz} + \partial_y \Pi_{yz}$ does not vanish in the presence of PA, up to the order of ε . In Ref. [6], this sum $\partial_x \Pi_{xz} + \partial_y \Pi_{yz}$ is also missing in the LHS of Eq. (2), which the authors employ as an extended GD relation in deriving their Eq. (5). In the present study, we use our Eq. (12), whose LHS includes $\partial_x \Pi_{xz} + \partial_y \Pi_{yz}$, as an extended GD relation to derive our formula for the thermal force density $\sigma_z^{(\text{th})}$ of Eq. (46), consistently with principles of linear nonequilibrium thermodynamics.

The superscript ^(th) is used to indicate a result in the linear regime for thermoosmosis. Replacing the integrand in Eq. (36) by $\sigma_z^{(\text{th})}(r_2)$ gives $v_z^{(\text{th})}(r)$. Integrating this result multiplied by $\rho^{(\text{ref})}$ over the tube's cross-section gives the total mass flow rate, for which we write $d\mathcal{M}_R^{(\text{th})}/(dt)$. Using the free-energy functional introduced in Section III C, we rewrite Eq. (46) and give an explicit expression of $d\mathcal{M}_R^{(\text{th})}/(dt)$ in Section III D. In the absence of PA, because Eq. (46) vanishes, $v_z^{(\text{th})}$ and $d\mathcal{M}_R^{(\text{th})}/(dt)$ vanish. Thus, in our formulation, thermoosmosis of a mixture occurs only in the presence of PA.

Setting $\delta T \neq 0$ and $\delta P = \delta c_a = 0$, we use Eqs. (3), (6), and (34) to obtain the mass flow rate of the component n in thermoosmosis as

$$\frac{d}{dt} \mathcal{M}_{nR}^{(\text{th})} = \frac{\delta T}{(T^{(0)})^2} \left[\rho_n^{(\text{ref})} \left(P^{(\text{ref})} L_{11} + \bar{H}_-^{(\text{ref})} L_{12} - L_{13} \right) \pm \frac{1}{2} \left(P^{(\text{ref})} L_{21} + \bar{H}_-^{(\text{ref})} L_{22} - L_{23} \right) \right], \quad (47)$$

where the upper (lower) sign is taken for $n = a$ (b) in the double sign. The sum of Eq. (47) over $n = a$ and b gives $d\mathcal{M}_R^{(\text{th})}/(dt)$. Rewriting the resultant sum with the aid of the formulas for L_{11} , L_{12} , and L_{13} shown in Section III A, we obtain the same expression of $d\mathcal{M}_R^{(\text{th})}/(dt)$ as derived in the way mentioned in the preceding paragraph.

C. Free-energy functional in the renormalized local functional theory

The reduced temperature τ is defined as $(T - T_c)/T_c$, and its characteristic magnitude τ_* is defined as $|T_* - T_c|/T_c$. The scaled reduced-temperature $\hat{\tau}$ is defined as τ/τ_* . In the one-phase region we consider, τ is positive near a upper consolute (UC) point and is negative near a lower consolute (LC) point [47–49]. Using the conventional notation, we write $\alpha, \beta, \gamma, \nu$, and η for the critical exponents for a mixture. We adopt $\nu = 0.630$ and $\eta = 0.0364$ [50]; the (hyper)scaling relations give $2\beta + \gamma = 3\nu = 2 - \alpha$ and $\gamma = \nu(2 - \eta)$. In an equilibrium mixture with $\psi = 0$, we have $\xi = \xi_0|\tau|^{-\nu}$ in the critical regime, where ξ_0 is a material constant.

Neglecting coupling between ρ and φ in f_{bulk} , we assume

$$f_{\text{bulk}} = -\frac{CT\tau^2}{2} + u_c - s_c T + f_-(\psi) + \frac{M_-}{2} |\nabla\psi|^2 + f_+(\rho). \quad (48)$$

Although the variable τ is dropped for conciseness, f_+ is a regular function of ρ and τ and f_- is a function of ψ and τ . The constants u_c and s_c represent the values of u and s at the critical point, respectively. The coefficient M_- is described later. In the critical regime, the singular contribution to C [31, 51] becomes equal to $2k_B\xi_0^{-3}|\tau|^{-\alpha}$ multiplied by a universal number, as mentioned at footnote 51 of Ref. [39].

The reference state considered here is obtained by changing T from the critical point with $P = P^{(\text{ref})}$ and $\psi = 0$ being fixed. The chemical potentials, $\mu_a^{(\text{ref})}$ and $\mu_b^{(\text{ref})}$, are tuned so that this change is realized. Thus, the φ dependent part for the bulk of a mixture in Eq. (15) can be obtained by coarse-graining the ψ^4 model up to ξ under no external field [39]. The bare model, given by Eq. (D1), is defined at a microscopic scale and identifies the fluctuations with spacial resolution much smaller than ξ . We can regard the coarse-grained average profile as maximizing the probability density functional coarse-grained up to ξ , assuming that thermal fluctuations are not significant after coarse-graining anymore [39]. This is consistent with the statement given at Eq. (15).

We assume no coupling between ρ and φ in Eq. (48) because ρ can be regarded as a constant approximately. The coefficient C involves the fluctuations of the internal-energy

density. Some details on these points are mentioned in Appendix D. As shown in Eq. (D1), we can define A_0 so that the bare ψ^4 model has a term $A_0\tau\psi^2/2$, which is positive in the one-phase region. Thus, A_0 is positive near a UC point, and is negative near a LC point [31]. The sign is maintained in the coarse-graining procedure. We use the coarse-grained result given by the renormalized local functional theory (RLFT) [39].

In the RLFT, ω is defined as $(\xi_0/\xi)^{1/\nu}$ and M_- is given by $k_B T C_1 \omega^{-\eta\nu}$ with $C_1 (> 0)$ being a material constant. The self-consistent condition, $\omega = |\tau| + C_2 \omega^{1-2\beta} \psi^2$, determines how ξ depends on τ and ψ , where the constant C_2 equals $3u^* C_1 \xi_0$. This condition gives

$$\tau_* = \left(\frac{\xi_0}{r_{\text{tube}}} \right)^{1/\nu} \quad \text{and} \quad \psi_* = \frac{\tau_*^\beta}{\sqrt{C_2}}. \quad (49)$$

Defining a dimensionless function \hat{f} as

$$\hat{f}(\hat{\psi}) = \frac{1}{2} \hat{\omega}^{\gamma-1} |\hat{\tau}| \hat{\psi}^2 + \frac{1}{12} \hat{\omega}^{\gamma-2\beta} \hat{\psi}^4, \quad (50)$$

where $\hat{\psi} \equiv \psi/\psi_*$, $\hat{\tau} \equiv \tau/\tau_*$, and $\hat{\omega} \equiv \omega/\tau_*$ are used, we have

$$f_-(\psi) + \frac{M_-}{2} |\nabla\psi|^2 = \mu_-^{(\text{ref})} \varphi + \frac{\mu_* \psi_* T}{T_*} \hat{f}(\hat{\psi}) + \frac{\mu_* \psi_* T}{2T_*} \hat{\omega}^{-\eta\nu} \left| r_{\text{tube}} \nabla \hat{\psi} \right|^2. \quad (51)$$

As already explained, $\mu_-^{(\text{ref})}$ is determined so that the reference state at T is realized, being dependent on T . The sum of the second and third terms on the RHS above is $k_B T$ multiplied by the coarse-grained result of the ψ^4 model under no external field, coming from the RLFT. The first term on the RHS of Eq. (50) originates from $A_0\tau\psi^2/2$. The self-consistent condition is rewritten as

$$\hat{\omega} = |\hat{\tau}| + \hat{\omega}^{1-2\beta} \hat{\psi}^2, \quad (52)$$

which means that $\hat{\omega}$ is a function of $\hat{\psi}$ and $\hat{\tau}$. It is even with respect to $\hat{\psi}$, and hence $\hat{f}(\hat{\psi})$ is an even function. The function $\hat{f}(\hat{\psi})$ also depends on $\hat{\tau}$, but the variable $\hat{\tau}$ is dropped for conciseness. The osmotic susceptibility χ is given by the inverse of the second partial derivative of f_- with respect to ψ , $1/f_-''(\psi)$; the prime indicates the differentiation with respect the variable given explicitly. The partial derivative $\partial\hat{f}/(\partial\hat{\tau})$, appearing in the later calculation, equals

$$\frac{\pm 1}{2} \hat{\omega}^{\gamma-1} \hat{\psi}^2 + \frac{\partial\hat{\omega}}{\partial\hat{\tau}} \left(\frac{\gamma-1}{2} \hat{\omega}^{\gamma-2} |\hat{\tau}| \hat{\psi}^2 + \frac{\gamma-2\beta}{12} \hat{\omega}^{\gamma-2\beta-1} \hat{\psi}^4 \right), \quad (53)$$

where Eq. (52) gives

$$\frac{\partial \hat{\omega}}{\partial \hat{\tau}} = \frac{\pm 1}{1 + (2\beta - 1)\hat{\omega}^{-2\beta}\hat{\psi}^2}. \quad (54)$$

The same sign as τ is taken in each double sign of these equations. The first term of Eq. (53) originates from the coarse-grained result of $A_0\psi^2/2$. Equation (52) gives $|\hat{\psi}|^{1/\beta} < \hat{\omega}$ and $|\hat{\tau}| < \hat{\omega}$. For $\hat{\psi} \neq 0$, the sign of Eq. (53), or that of $\partial \hat{f}/(\partial \hat{\tau})$, coincides with that of τ , considering $\beta = 0.326$ and $\gamma = 1.24$. If $|\hat{\tau}|$ is much smaller than $\hat{\omega}$, Eq. (52) gives $|\hat{\psi}|^{1/\beta} \approx \hat{\omega}$ and thus Eq. (54) is approximately equal to $\pm 1/(2\beta)$. Then, in Eq. (53), the first term is found to be dominant over the rest. If $|\hat{\tau}|$ is close to $\hat{\omega}$, Eq. (54) is found to be close to ± 1 with the aid of Eq. (52). Then, the first term remains dominant in Eq. (53), accounting for approximately 80% of the total owing to the numerator $\gamma - 1 = 0.24$ in the parentheses.

We assume f_{surf} to be a linear function of φ , or ψ , as usual in studying the PA [25, 39]. The surface field h is defined as the negative of the coefficient of ψ . This assumption and this definition are involved in calculating the equilibrium profile, which is used in Section IV. The calculation procedure is mentioned below Eq. (15) and is the same as that of Ref. [39]. Applying Eqs. (48) and (51), we find that $\hat{\psi}^{(0)}(\hat{r})$ is the solution of

$$0 = \hat{f}'(\hat{\psi}) - \frac{1}{2} \frac{\partial \hat{\omega}^{-\eta\nu}}{\partial \hat{\psi}} \left(\partial_{\hat{r}} \hat{\psi} \right)^2 - \hat{\omega}^{-\eta\nu} \left(\partial_{\hat{r}}^2 + \frac{1}{\hat{r}} \partial_{\hat{r}} \right) \hat{\psi} \quad \text{for } \hat{r} < 1, \quad (55)$$

together with the boundary condition at the wall, $(\hat{\psi}^{(0)})'(1) = \hat{h}\hat{\omega}^{\eta\nu}$. Here, $\hat{\omega}$ is regarded as a function of $\hat{\psi}$ and $\hat{\tau}$ via Eq. (52) and a scaled surface field \hat{h} is defined as $hT_*/(T\mu_*r_{\text{tube}})$. These equations are shown in Appendix D of Ref. [20]; $\hat{\psi}^{(0)}$ is totally determined by $|\hat{\tau}|$ and \hat{h} . If we change the sign of \hat{h} , the sign of $\hat{\psi}^{(0)}$ changes with the magnitude remaining the same. Notably, $|h|$ represents the strength of the PA and vanishes in its absence.

D. Formulas incorporating the RLFT

We apply Eq. (48) and the results of the RLFT to rewrite the RHS of Eq. (46). Owing to Eqs. (20) and (51), we have

$$u^{(0)} - u^{(\text{ref})} = -\frac{(T^{(0)})^2 \mu_* \psi_*}{T_c T_*} \frac{\partial}{\partial \tau} \left(\hat{f} + \frac{\hat{\omega}^{-\eta\nu}}{2} \left| \partial_{\hat{r}} \hat{\psi}^{(0)} \right|^2 \right) + \bar{H}_-^{(\text{ref})} \psi^{(0)}, \quad (56)$$

where the partial derivative with respect to τ is done with $\hat{\psi}$ fixed and is evaluated at $\varepsilon = 0$. The first term on the RHS represents the difference in the internal energy density involved

in the coarse-grained result of the ψ^4 model. In deriving the second term, we drop one term, which is proportional to the thermal expansion coefficient. This term gives negligibly small contribution to our later numerical results, as described in Appendix E. Owing to Eqs. (11), (48), and (51), we have

$$P^{(0)} - P^{(\text{ref})} = -\frac{\mu_*\psi_*T^{(0)}}{T_*} \left(\hat{f} + \frac{\hat{\omega}^{-\eta\nu}}{2} \left| \partial_{\hat{r}} \hat{\psi} \right|^2 \right). \quad (57)$$

We define a scaled thermal force density, $\hat{\sigma}_z^{(\text{th})}$, so that Eq. (46) is rewritten as

$$\sigma_z^{(\text{th})}(\hat{r}r_{\text{tube}}) = \frac{\mu_*\psi_*\delta T}{\tau_*T_*L_{\text{tube}}} \hat{\sigma}_z^{(\text{th})}(\hat{r}), \quad (58)$$

and have

$$\hat{\sigma}_z^{(\text{th})} = \tau_* \left(\hat{f} + \frac{1}{2\hat{\omega}^{\eta\nu}} \left| \partial_{\hat{r}} \hat{\psi} \right|^2 \right) + \frac{T^{(0)}}{T_c} \left(\frac{\partial \hat{f}}{\partial \hat{\tau}} - \frac{\eta\nu}{2\hat{\omega}^{\eta\nu+1}} \frac{\partial \hat{\omega}}{\partial \hat{\tau}} \left| \partial_{\hat{r}} \hat{\psi} \right|^2 \right), \quad (59)$$

which is evaluated at $\varepsilon = 0$. The first term on the RHS of Eq. (59) comes from Eq. (57), whereas the second term comes from the first term on the RHS of Eq. (56). The last term in the parentheses of Eq. (46) cancels out the last term on the RHS of Eq. (56). Thanks to this cancellation, the thermal force density does not involve $\bar{H}_-^{(\text{ref})}$. Except for the factors τ_* and $T^{(0)}/T_c$, Eq. (59) is determined by the scaled reduced-temperature $\hat{\tau}$ and the magnitude of the scaled surface field $|\hat{h}|$ in the framework of the RLFT. The magnitude of the sum in the second parentheses, in particular, is determined by $|\hat{\tau}|$ and $|\hat{h}|$ owing to Eqs. (53) and (54).

As mentioned in Section III B, $\varepsilon v_z^{(1)}$ in thermoosmosis is given by

$$v_z^{(\text{th})}(\hat{r}r_{\text{tube}}) = \frac{8\mathcal{I}_*\delta T}{T_*\tau_*\pi r_{\text{tube}}^2} \int_{\hat{r}}^1 d\hat{r}_1 \frac{1}{\hat{r}_1\hat{\eta}(\hat{r}_1)} \int_0^{\hat{r}_1} d\hat{r}_2 \hat{r}_2 \hat{\sigma}_z^{(\text{th})} \quad (60)$$

in the tube, whereas the total mass flow rate in thermoosmosis is given by

$$\frac{d\mathcal{M}_{\text{R}}^{(\text{th})}}{dt} = \frac{\rho^{(\text{ref})}\mathcal{I}_*\delta T}{T_*\tau_*} \Omega [1, \hat{\sigma}_z^{(\text{th})}], \quad (61)$$

which is proportional to δT . The constant of proportionality represents the thermoosmotic conductance. We define the dimensionless thermoosmotic conductance, denoted by $\hat{G}^{(\text{th})}$, as the quotient of the constant divided by $\rho^{(\text{ref})}\mathcal{I}_*/(T_*\tau_*)$, and have

$$\hat{G}^{(\text{th})} = \Omega [1, \hat{\sigma}_z^{(\text{th})}]. \quad (62)$$

If we change the sign of \hat{h} , $\hat{\sigma}_z^{(\text{th})}(\hat{r})$ remains the same and is independent of which component is adsorbed onto the tube's wall. However, it is not the case with $v_z^{(\text{th})}$ of Eq. (60), $d\mathcal{M}_R^{(\text{th})}/(dt)$ of Eq. (61), and $\hat{G}^{(\text{th})}$ of Eq. (62) because $\hat{\eta}$ is not always an even function of $\hat{\psi}$.

Some of the formulas of the Onsager coefficients are simplified using Eq. (48) and the results of the RLFT. We have $\hat{f}''(0) = |\hat{\tau}|^\gamma$ and

$$f_-''(0) = \frac{k_B T C_2 |\tau|^\gamma}{3u^* \xi_0^3}. \quad (63)$$

Because of Eq. (48), we can replace χ in Eq. (33) with $1/f_-''(\psi)$. By definition, we have

$$\Lambda_* = \frac{3u^* R T_c \xi_0^2 T_*^{\nu-\gamma}}{C_2 T_* \eta_*}. \quad (64)$$

We write z_ψ for the dynamic critical exponent for the order-parameter fluctuations and use $z_\psi = 3.067$ [52, 53]. With the aid of the result of the dynamic renormalization-group calculation [29, 30, 32], we have

$$\hat{\Lambda} = \hat{\omega}^{\nu(z_\psi-2)} \left[\hat{f}''(\hat{\psi}) \right]^{-1} \quad (65)$$

evaluated at $\varepsilon = 0$, as described in Appendix E of Ref. [20]. Using Eq. (33) with $R = 1/(6\pi)$ and Eq. (65), we can rewrite the second term on the RHS of Eq. (41) as

$$\frac{\mathcal{I}_* \psi_* T^{(0)}}{\mu_*} \frac{16\pi T_c}{9T^{(0)}} \int_0^1 d\hat{r} \hat{r} \hat{\Lambda}(\hat{r}), \quad (66)$$

which is essentially the same as obtained in Ref. [20]. Likewise, in the second terms on the RHS of the new formulas (44) and (45), the coefficients multiplied by the integrals are respectively rewritten as

$$\mathcal{I}_* \psi_* T^{(0)} \frac{16\pi T_c}{9T^{(0)}} \quad \text{and} \quad \mathcal{I}_* \mu_* \psi_* T^{(0)} \frac{16\pi T_c}{9T^{(0)}}. \quad (67)$$

The integrals can be calculated if $\hat{H}_-^{(0)}$ is known. To calculate $\hat{Y}^{(0)}$ contained in the first terms on the RHS's of Eqs. (43)–(45), we can use Eq. (56), which involves $\bar{H}_-^{(\text{ref})}$. Thus, it is necessary to know how \bar{H}_- depends on φ to calculate these integrals and terms. We can calculate the dependence in such a theoretical framework as used in Refs. [54–56].

IV. NUMERICAL RESULTS OF THERMOOSMOSIS

In this section, we study thermoosmosis numerically with the aid of the formulas in Section IIID and the software Mathematica (Wolfram Research), supposing a mixture

mixture	T_c [K]	ξ_0 [nm]	$\tau_* \times 10^5$	C_2 [cm ⁶ /g ²]	ψ_* [g/cm ³]	μ_* [cm ² /s ²]	η_* [mPa·s]
LW	307	0.198	5.12	0.714	0.0470	137	2.44
NEMP	300	0.230	6.49	1.05	0.0419	150	0.510

TABLE I: Parameter values: Origins of the values are described in the text.

of 2,6-lutidine and water (LW) near the LC point and a mixture of nitroethane and 3-methylpentane (NEMP) near the UC point. In each mixture, the former (latter) component is taken to be the component a (b). The tube radius r_{tube} is set to $0.1 \mu\text{m}$. The parameter values we use are listed in Table I and are the same as used in Ref. [20]. The values of ξ_0 are taken from the experimental data of Refs. [45, 57]. The first entry of Eq. (49) gives the values of τ_* , which appears in Eq. (59). In Appendix C of Ref. [20], we estimate C_2 from the data of Refs. [58, 59]. The second entry of Eq. (49) gives the value of ψ_* , and then Eq. (37) gives that of μ_* . In Appendix E of Ref. [20], we obtain the viscosity as a function of the reduced temperature and the order parameter [60, 61] and find the value of η_* from the data of Refs. [57, 62–64]. These values give $\mathcal{I}_* L_{\text{tube}} = 1.04 \times 10^{-2} \mu\text{m}^4/\text{s}$ ($4.84 \times 10^{-2} \mu\text{m}^4/\text{s}$) for a mixture of LW (NEMP). The magnitude of the surface field h should be smaller than approximately $10 \text{ cm}^3/\text{s}^2$ when 2,6-lutidine adsorbs onto the solid surface, according to the discussion in Section 6 of Ref. [27]. We mainly use $\hat{h} = 73.0$ (66.6) for a mixture of LW (NEMP), which amounts to $h \approx 0.1 \text{ cm}^3/\text{s}^2$.

A. Equilibrium profile and thermal force density

Equilibrium profiles in the tube are shown in Fig. 2. Because of $\hat{h} > 0$, $\hat{\psi}^{(0)}(\hat{r})$ increases, or the component a is more concentrated, near the wall at $\hat{r} = 1$. For each mixture, $\hat{\psi}^{(0)}(\hat{r})$ is larger at the smaller value of $|\tau|$, since the adsorption layer extends towards the tube's center as the critical temperature is approached. At $|\tau| = 3.2 \times 10^{-3}$, the adsorption layer appears to localize near the tube's wall, and $\hat{\psi}^{(0)}(\hat{r})$ is larger for a mixture of NEMP than for a mixture of LW in the whole region of $0 \leq \hat{r} \leq 1$ although the difference is hard to see for $\hat{r} < 0.7$ and $\hat{r} = 1$ in the figure. This magnitude relationship is reasonable considering that $|\hat{\tau}|$ is smaller for a mixture of NEMP. At $|\tau| = 1.25 \times 10^{-5}$,

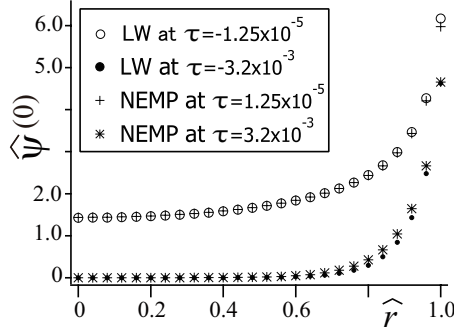


FIG. 2: Plots of the dimensionless order parameter at equilibrium, $\hat{\psi}^{(0)}(\hat{r})$, against the dimensionless radial distance \hat{r} . The surface field is set to $h = 0.1 \text{ cm}^3/\text{s}^2$. For a mixture of LW (NEMP), open circles (crosses) represent $\hat{\psi}^{(0)}(\hat{r})$ at $|\tau| = 1.25 \times 10^{-5}$, whereas closed circles (asterisks) represent $\hat{\psi}^{(0)}(\hat{r})$ at $|\tau| = 3.2 \times 10^{-3}$. We use the values of τ_* in Table I to find $\hat{r} = -0.24$ (0.19) for open circles (crosses), and $\hat{r} = -63$ (49) for closed circles (asterisks).

the relationship holds only for $\hat{r} < 0.7$, and ξ at $\psi = 0$, given by $\xi_0|\tau|^{-\nu}$, exceeds the tube radius. It is approximately equal to $2r_{\text{tube}}$ at $|\tau| = 1.25 \times 10^{-5}$ while to $r_{\text{tube}}/10$ at $|\tau| = 3.2 \times 10^{-3}$ for both mixtures. At $\hat{r} = 0$ under $|\tau| = 1.25 \times 10^{-5}$, the composition is definitely off-critical and ξ becomes approximately equal to $r_{\text{tube}}/2$ for both mixtures.

Circles in Fig. 3 represent $\hat{\sigma}_z^{(\text{th})}$ of Eq. (59) at $|\tau| = 1.25 \times 10^{-5}$. Hereafter, $\tau(\hat{r})$ represents the (scaled) reduced temperature in the reference state. Figures 3(a) and 3(b) show that the thermal force density becomes remarkable near the tube's wall. The first term of Eq. (53), which originates from $A_0\psi^2/2$ in the term of ψ squared in the bare model, contributes to the second term on the RHS of Eq. (59) via the term $\partial\hat{f}/(\partial\hat{r})$. Crosses in Fig. 3 represent this contribution, which is denoted by $\hat{\sigma}_z^{(\text{sq})}$ and is given by

$$\hat{\sigma}_z^{(\text{sq})}(\hat{r}) = \pm \frac{T^{(0)}}{2T_c} \hat{\omega}^{\gamma-1} \hat{\psi}^2. \quad (68)$$

This is evaluated at $\varepsilon = 0$ with the same sign as τ being taken. This sign for $\hat{\psi} \neq 0$ comes from that of A_0 , which is negative (positive) for the LC (UC) point. The rest in the second term on the RHS of Eq. (59) is plotted with triangles. The first term on the RHS of Eq. (59), which originates from the scalar-pressure deviation Eq. (57), is plotted with squares. This term gives negligibly small contributions to $\hat{\sigma}_z^{(\text{th})}$ in the whole region of \hat{r} . It remains the case for $|\tau|$ up to 6.4×10^{-3} although data are not shown. This can be expected because the first

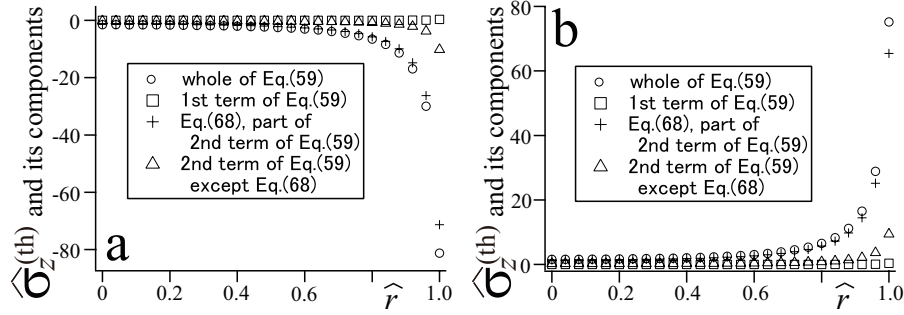


FIG. 3: Plots of the scaled thermal force density, $\hat{\sigma}_z^{(\text{th})}$, and its components against the dimensionless radial distance \hat{r} at $|\tau| = 1.25 \times 10^{-5}$ for a mixture of LW (a) and a mixture of NEMP (b). Here, the reduced temperature τ is evaluated at $T = T^{(0)}$, and is negative (positive) in the former (latter) mixture. The surface field is set to $h = 0.1 \text{ cm}^3/\text{s}^2$. Circles represent $\hat{\sigma}_z^{(\text{th})}$ of Eq. (59), whereas squares represent its first term. Its second term can be separated into two parts; $\hat{\sigma}_z^{(\text{sq})}$ of Eq. (68) and the rest. Crosses represent the former, whereas triangles represent the latter.

term contains a small positive factor τ_* . Near the wall in Fig. 3, we can see that $\hat{\sigma}_z^{(\text{sq})}(\hat{r})$ is dominant in $\hat{\sigma}_z^{(\text{th})}(\hat{r})$. The ratio $\hat{\sigma}_z^{(\text{sq})}(\hat{r})/\hat{\sigma}_z^{(\text{th})}(\hat{r})$ at $\hat{r} = 1$ is 0.88 (0.87) for $|\tau| = 1.25 \times 10^{-5}$ in a mixture of LW (NEMP). At $|\tau| = 3.2 \times 10^{-3}$, the ratio at $\hat{r} = 1$ remains approximately the same, 0.86 (0.85), although each of $\hat{\sigma}_z^{(\text{sq})}(\hat{r})$ and $\hat{\sigma}_z^{(\text{th})}(\hat{r})$ at $\hat{r} = 1$ is roughly halved.

In Fig. 4 for a mixture of NEMP, $\hat{\sigma}_z^{(\text{sq})}(\hat{r})$ and $\hat{\sigma}_z^{(\text{th})}(\hat{r})$ become distinctly larger near the wall as τ is smaller and h is larger. For various values of $|\tau|$ and h examined in Figs. 3 and 4, over the whole region of \hat{r} , the ratio $\hat{\sigma}_z^{(\text{sq})}(\hat{r})/\hat{\sigma}_z^{(\text{th})}(\hat{r})$ remains approximately the same as the ratio at $\hat{r} = 1$. Thus, as far as examined, over the whole region of \hat{r} , $\hat{\sigma}_z^{(\text{th})}(\hat{r})$ is negative (positive) in a mixture of LW (NEMP) and is contributed dominantly from $\hat{\sigma}_z^{(\text{sq})}(\hat{r})$. In each inset of Fig. 4, $\hat{\psi}^{(0)}(\hat{r})$ increase more steeply near the wall as h is larger, like $\hat{\sigma}_z^{(\text{th})}(\hat{r})$ in the main figure. For each value of h in Figs. 4(a) and 4(b), as \hat{r} decreases, both $\hat{\psi}^{(0)}(\hat{r})$ and $\hat{\sigma}_z^{(\text{th})}(\hat{r})$ decrease more gradually at the smaller value of τ . These behaviors can be explained by the dominance of Eq. (68). The dominance of Eq. (68) in the term involving $\partial\hat{f}/(\partial\tau)$ on the RHS of Eq. (59) is expected from approximate estimation mentioned below Eq. (54).

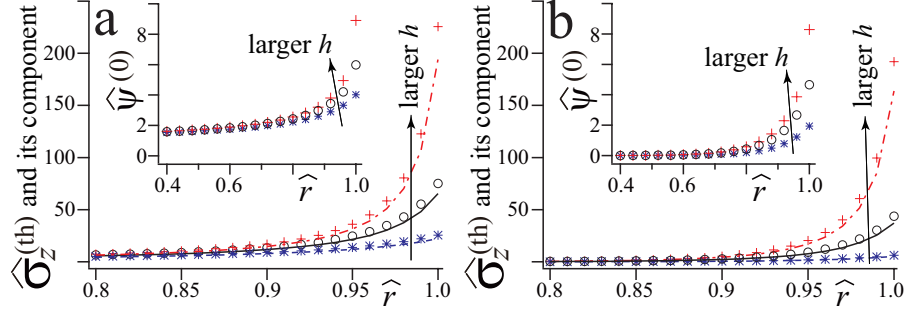


FIG. 4: Plots of the scaled thermal force density, $\hat{\sigma}_z^{(th)}$, and its dominant term $\hat{\sigma}_z^{(sq)}$ against the dimensionless radial distance $\hat{r} (\geq 0.8)$ for a mixture of NEMP. The reduced temperature τ evaluated at $T = T^{(0)}$ is 1.25×10^{-5} in (a) and 3.2×10^{-3} in (b). The surface field h is set to $10^{-1} \text{ cm}^3/\text{s}^2$ for circles ($\hat{\sigma}_z^{(th)}$) and solid curves ($\hat{\sigma}_z^{(sq)}$); these results in (a) are already shown in Fig. 3(b). Setting h to $10^{-0.5}$ ($10^{-1.5}$) cm^3/s^2 , we obtain results shown by red crosses and dash-dot curves (blue asterisks and dashed curves); symbols represent $\hat{\sigma}_z^{(th)}$ and curves represent $\hat{\sigma}_z^{(sq)}$. The change of h is indicated by arrows. (Insets) Plots of the dimensionless order parameter at equilibrium, $\hat{\psi}^{(0)}(\hat{r})$, against $\hat{r} (\geq 0.4)$. The parameter values for each symbol are the same as those for the same symbol in the main figure in each of (a) and (b). The results of the circles are already shown in Fig. 2.

B. Velocity field and conductance

We define $\hat{v}_z^{(th)}(\hat{r})$ as the double integral of Eq. (60), which is plotted in Fig. 5. When δT is positive, $\hat{v}_z^{(th)}$ has the same sign as $v_z^{(th)}$. At $|\tau| = 3.2 \times 10^{-3}$, $\hat{v}_z^{(th)}(\hat{r})$ changes only for $\hat{r} > 0.8$ and the velocity appears to slip across a narrow region near the wall. This is because, as shown in Fig. 4(b), the adsorption layer and the thermal force density localize sharply in a region near the wall $\hat{r} > 0.8$. The slip velocity is given by $\hat{v}_z^{(th)}(0)$, which is -0.042 (0.061) for a mixture of LW (NEMP) at $h = 0.1 \text{ cm}^3/\text{s}^2$. Converting the value to the slip velocity with dimensions, we find it to be -7.09 (38.2) $(\mu\text{m})^2/(\text{s}\cdot\text{K})$ multiplied by $\delta T/L_{\text{tube}}$, which is comparable in magnitude with typical thermophoretic mobility far from the critical point [7, 65–67]. For each value of h in Fig. 5, $|\hat{v}_z^{(th)}(\hat{r})|$ at $|\tau| = 1.25 \times 10^{-5}$ is larger than $|\hat{v}_z^{(th)}(\hat{r})|$ at $|\tau| = 3.2 \times 10^{-3}$ inside the tube and increases gradually in magnitude as \hat{r} decreases without showing an obvious slip. In Fig. 5(b), $\hat{v}_z^{(th)}(\hat{r})$ increases with h inside the tube, as expected. The spatial resolution of our formulation is given

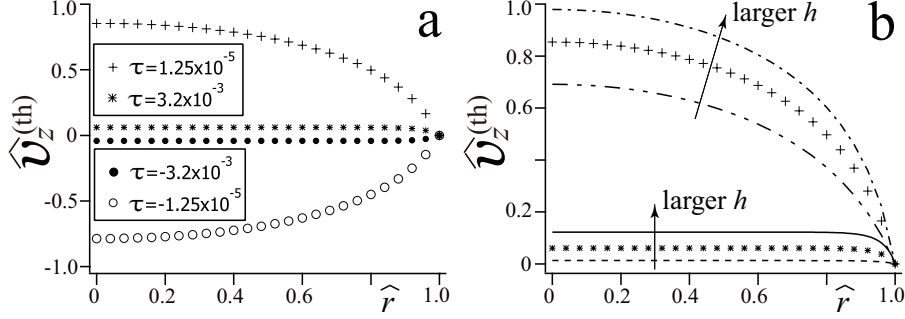


FIG. 5: The z component of the dimensionless velocity in thermoosmosis, $\hat{v}_z^{(\text{th})}(\hat{r})$, is plotted against the dimensionless radial distance \hat{r} . (a) Closed and open circles represent $\hat{v}_z^{(\text{th})}(\hat{r})$ for a mixture of LW at $\tau = -3.2 \times 10^{-3}$ and -1.25×10^{-5} , respectively. The reduced temperature τ is evaluated at $T = T^{(0)}$. Asterisks and crosses represent $\hat{v}_z^{(\text{th})}(\hat{r})$ for a mixture of NEMP at $\tau = 3.2 \times 10^{-3}$ and 1.25×10^{-5} , respectively. The surface field is set to $h = 10^{-1}$ cm³/s². (b) Asterisks and crosses represent the same results as those in (a), respectively. The solid curve (the dashed curve) represents $\hat{v}_z^{(\text{th})}(\hat{r})$ for a mixture of NEMP at $\tau = 3.2 \times 10^{-3}$ with h set to $10^{-0.5}$ ($10^{-1.5}$) cm³/s². The dash-dot curve (the dash-dot-dot curve) represents $\hat{v}_z^{(\text{th})}(\hat{r})$ at $\tau = 1.25 \times 10^{-5}$ with h set to $10^{-0.5}$ ($10^{-1.5}$) cm³/s². The change of h is indicated by arrows.

by ξ . For $h = 0.1$ cm³/s² and $|\tau| = 1.25 \times 10^{-5}$ (3.2×10^{-3}), a mixture of LW has $\xi/r_{\text{tube}} = 0.030$ (0.036) and a mixture of NEMP has 0.032 (0.038) at $\hat{r} = 1$. With the spatial resolution given by these values, one would trace rapid changes of $\hat{v}_z^{(\text{th})}$ near the wall shown in Fig. 5. In passing, the slip velocity at $|\tau| = 3.2 \times 10^{-3}$ can be evaluated approximately using the Gaussian model mentioned in Appendix F.

The dimensionless thermoosmotic conductance is defined at Eq. (62), which is rewritten as

$$\hat{G}^{(\text{th})} = 16 \int_0^1 d\hat{r} \hat{r} \hat{v}_z^{(\text{th})}(\hat{r}). \quad (69)$$

When δT is positive, $\sigma_z^{(\text{th})}(\hat{r})$ has the same sign as $\hat{\sigma}_z^{(\text{th})}(\hat{r})$. For each mixture in our numerical results, the sign of $\hat{\sigma}_z^{(\text{th})}(\hat{r})$ remains the same for $0 \leq \hat{r} \leq 1$, and thus is the same as that of $\hat{v}_z^{(\text{th})}(\hat{r})$ and that of $\hat{G}^{(\text{th})}$; $\hat{G}^{(\text{th})} > 0$ (< 0) means that the flow direction is the same as (opposite to) the direction of the temperature gradient. Thus, according to our numerical results, a mixture of NEMP near the UC point flows towards the reservoir with the higher temperature, whereas a mixture of LW near the LC point flows in the opposite

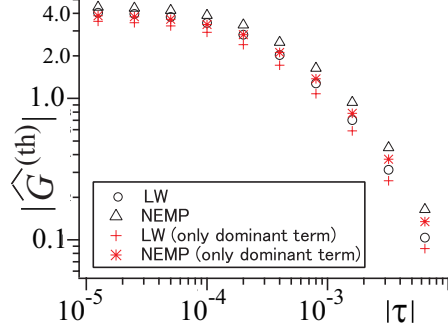


FIG. 6: Logarithmic plots of the absolute value of the dimensionless thermoosmotic conductance against that of the reduced temperature $|\tau|$, evaluated at $T = T^{(0)}$, for a mixture of LW (circle) and a mixture of NEMP (triangle) with the surface field set to $h = 0.1 \text{ cm}^3/\text{s}^2$. The dimensionless conductance, $\hat{G}^{(\text{th})} = \Omega[1, \hat{\sigma}_z^{(\text{th})}]$ of Eq. (62) or (69), is negative for a mixture of LW, whereas positive for a mixture of NEMP. Red crosses (asterisks) represent $\Omega[1, \hat{\sigma}_z^{(\text{sq})}]$, which is dominant in $\hat{G}^{(\text{th})}$, for a mixture of LW (NEMP).

direction. This is independent of which component is adsorbed onto the tube's wall owing to the independence of Eq. (59) from the sign of h .

Logarithmic plots of $|\hat{G}^{(\text{th})}|$ against $|\tau|$ are shown in Fig. 6, where the conductance increases in magnitude as $|\tau|$ decreases. This is because larger susceptibility makes the PA stronger. For smaller values of $|\tau|$, the increase becomes more gradual. This would represent effect of the size of the tube, considering that the value of ξ at $\psi = 0$, given by $\xi_0|\tau|^{-\nu}$, exceeds the tube radius approximately for $|\tau| < 5 \times 10^{-5}$. Equation (68), $\hat{\sigma}_z^{(\text{sq})}$, contributes to $\hat{G}^{(\text{th})}$ dominantly in the range of τ examined in Fig. 6. Changing the value of h for a mixture of NEMP, we calculate the conductance, as shown in Fig. 7. As h increases, $\hat{G}^{(\text{th})}$ increases, as expected since $\hat{\psi}^{(0)}$, $\hat{\sigma}_z^{(\text{th})}$, and $\hat{v}_z^{(\text{th})}$ then increase in Figs. 4 and 5(b). In Fig. 7(b), $\hat{G}^{(\text{th})}$ becomes less dependent on h in logarithmic scale as τ decreases. This tendency is also observed for the dependence of $\hat{v}_z^{(\text{th})}$ on h in Fig. 5(b). The contribution from $\hat{\sigma}_z^{(\text{sq})}$ to $\hat{G}^{(\text{th})}$ remains dominant for the values of τ and \hat{h} examined in Fig. 7(b).

C. Prediction of universal properties

As mentioned below Eq. (68), in our numerical results, the first term on the RHS of

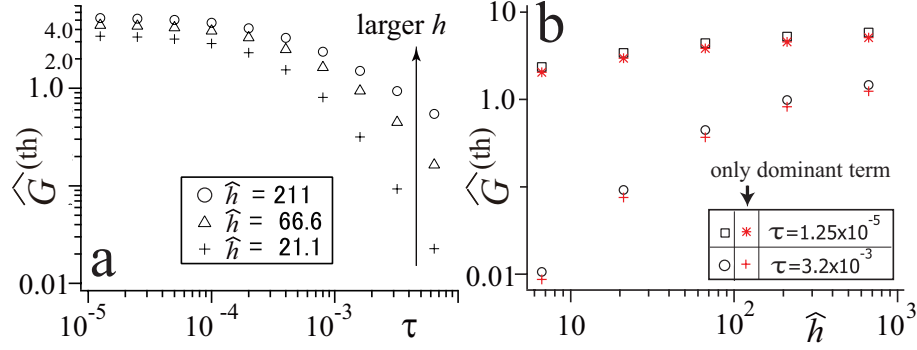


FIG. 7: (a) Logarithmic plots of the dimensionless thermoosmotic conductance, $\hat{G}^{(th)}$ against the reduced temperature τ , evaluated at $T = T^{(0)}$, for a mixture of NEMP. Triangles in this figure and in Fig. 6 represent the same results with the surface field set to $h = 10^{-1} \text{ cm}^3/\text{s}^2$. Circles (crosses) represent $\hat{G}^{(th)}$ for $h=10^{-0.5}$ ($10^{-1.5}$) cm^3/s^2 . The corresponding values of the scaled surface field \hat{h} are shown in the figure; the change of h is indicated by an arrow. (b) Logarithmic plots of $\hat{G}^{(th)}$ against the scaled surface field \hat{h} for a mixture of NEMP. Squares and circles represent $\hat{G}^{(th)} = \Omega[1, \hat{\sigma}_z^{(th)}]$ at $\tau = 1.25 \times 10^{-5}$ and 3.2×10^{-3} , respectively. The values of τ are evaluated at $T = T^{(0)}$. Red asterisks (crosses) represent $\Omega[1, \hat{\sigma}_z^{(sq)}]$, which is dominant in $\hat{G}^{(th)}$, at $\tau = 1.25 \times 10^{-5}$ (3.2×10^{-3}). The change of τ is indicated by an arrow.

Eq. (59) is negligible. This would be mainly because it contains a very small positive factor τ_* (Table I). Thus, owing to $T_c \approx T^{(0)}$, it is strongly suggested that

$$\hat{\sigma}_z^{(th)} \approx \frac{\partial \hat{f}}{\partial \hat{\tau}} - \frac{\eta\nu}{2\hat{\omega}^{\eta\nu+1}} \frac{\partial \hat{\omega}}{\partial \hat{\tau}} \left| \partial_{\hat{r}} \hat{\psi} \right|^2, \quad (70)$$

which is evaluated at $\varepsilon = 0$, holds for any mixture. The RHS of Eq. (70) is free from the material constants, *i.e.* does not suppose a special mixture, because it is determined only by the scaled reduced-temperature $\hat{\tau}$ and the magnitude of the scaled surface field $|\hat{h}|$. Using various values of $(\hat{\tau}, \hat{h})$, we numerically find that Eq. (68) is dominant in $\hat{\sigma}_z^{(th)}$. In this sense, we have

$$\hat{\sigma}_z^{(th)} \approx \pm \frac{\hat{\omega}^{\gamma-1}}{2} \hat{\psi}^2 \quad (71)$$

evaluated at $\varepsilon = 0$, where the sign is taken as that of τ , *i.e.*, as that of A_0 in the bare model. Notably, Eq. (71) is strongly expected to hold in the critical regime for any mixture, which is also supported by the approximate estimation given below Eq. (54) and by the results in Figs. 6 and 7(b). Therefore, we can predict that, for any mixture near the UC (LC) point,

the direction of thermoosmosis is the same as (opposite to) that of the temperature gradient, irrespective of which component is adsorbed onto the wall, if the critical composition is kept in the middle of each reservoir.

V. FURTHER DISCUSSION AND SUMMARY

Our numerical results are based on the calculation up to the order of ε , or in the linear regime with respect to δT . Obviously, after a temperature difference δT is imposed between the reservoirs, the deviation of τ from the value of τ at $T = T^{(0)}$ is required to be much smaller in magnitude than the value at $T = T^{(0)}$ throughout inside the tube. For example, if the latter value is set to 10^{-3} in magnitude, we may set $|\delta T|/T_c$ to be smaller than its 10 %, 10^{-4} . The resultant local changes of T and $\hat{\psi}$ shift $\hat{\sigma}_z^{(\text{th})}$. As far as examined, the shift is roughly smaller than 10 % in the adsorption layer. For $|\delta T| = 100 \text{ mK} \ll |T^{(0)} - T_c| \approx 1 \text{ K}$ and $L_{\text{tube}} = 10 \text{ }\mu\text{m}$, we find from the results in Fig. 5(a) that the slip velocity is approximately $0.1 \text{ }\mu\text{m/s}$, which would be measured experimentally. In passing, in the experiments on the Brownian motion of colloidal particles in a mixture, $|\tau|$ is set to be smaller than 10^{-4} homogeneously [68, 69].

The RLFT succeeds in describing several phenomena of a mixture [39]. However, in the theory, crossover to the regular part of the free energy [54–56, 70–72] is not considered, the results up to the one-loop order approximation are used, and validity of the definition of the local correlation length in the inhomogeneous composition is not fully discussed. The regular parts of the transport coefficients [73] are considered only for the viscosity η_s , whose singularity is very weak, in the present study. These points are to be improved in future for quantitatively better numerical results for transport properties, not only of thermoosmosis but also of various phenomena, such as cross effects, described by the Onsager coefficients. Still, the qualitative property on the flow direction in thermoosmosis of a mixture, predicted by the present study, should be robust to changes of details in the formulation, considering that it originates from the sign of the coefficient, A_0 , in the bare model.

Equation (71) leads to a possible power-law dependence with respect to $|\tau|$ for the slip velocity far from a flat wall in thermoosmosis, as shown in Appendix F. Thermophoresis

would occur for a particle in a mixture in the presence of PA onto the particle surface; the direction of the particle motion is expected to be the same as (opposite to) that of the imposed temperature gradient if the mixture is near the LC (UC) point and has the the critical composition far from the particle. These points clearly require further investigation in future.

Our present study is summarized as follows. We consider transport of a binary fluid mixture, lying in the one-phase region near the demixing critical point, through a capillary tube. One component is assumed to be adsorbed onto the tube’s adiabatic wall and the adsorption layer can be much thicker than the molecular size. We formulate the hydrodynamics from a coarse-grained free-energy functional using an extended Gibbs-Duhem relation, Eq. (12), consistently with principles of linear nonequilibrium thermodynamics. This relation is originally derived in Ref. [37], and is derived on a more general condition in Appendix A. Assuming the critical composition in the middle of each reservoir in the reference equilibrium state, we derive the Onsager coefficients in Section III A. Among various phenomena described by the coefficients, we focus on thermoosmosis of a mixture. The formula for the thermal force density, Eq. (46), is explicitly derived as an extension of Derjaguin and Sidorenkov’s formula for one-component fluids and is rewritten as Eq. (59) in terms of the renormalized local functional theory [33, 39]. We predict that the direction of thermoosmotic flow of a mixture near the upper (lower) consolute point is the same as (opposite to) that of the temperature gradient, irrespective of which component is adsorbed onto the tube’s wall. The magnitude of the thermoosmotic conductance increases, with the increase being more gradual owing to the size effect, as the critical point is approached. The thermal force density is given in a scaled form by Eq. (70), which depends only on the scaled reduced-temperature and the scaled surface field, and is dominantly contributed from Eq. (71).

Such mesoscopic inhomogeneity as is generated in a mixture by the surface field can occur in many soft matter systems — polymer solutions, polyelectrolytes, and liquid crystals [31, 74]. In particular, their dynamics driven by a temperature gradient would be studied by applying our procedure to a suitable set of hydrodynamic equations based on a coarse-grained free-energy functional. Also, for thermoosmosis of a solution far from the critical point, our results may help as a guide regarding properties independent of the microscopic details.

Hence, our present study would lay solid foundations on non-isothermal hydrodynamics in the presence of mesoscopic inhomogeneity and predict universal properties on thermoosmosis of a near-critical binary fluid mixture.

Appendix A: Non-dissipative part of the stress tensor

For conciseness, we here write $(T, \rho_n, \nabla \rho_n)$ for the variables of f_{bulk} in Eq. (8). They are also variables of s and u because of Eq. (20). The entropy density is also a function of u , ρ_n , and $\nabla \rho_n$, and we define \tilde{s} so that

$$s(T, \rho_n, \nabla \rho_n) = \tilde{s}(u(T, \rho_n, \nabla \rho_n), \rho_n, \nabla \rho_n) \quad (\text{A1})$$

holds. Explicit expressions of \tilde{s} , although given in special cases [37, 38], are not required in a general argument given below. We have

$$\frac{\partial \tilde{s}}{\partial u} = \frac{1}{T} \quad \text{and} \quad \frac{\partial \tilde{s}}{\partial \zeta} = -\frac{1}{T} \frac{\partial f_{\text{bulk}}}{\partial \zeta} \quad (\text{A2})$$

for $\zeta = \rho_n$ or $\nabla \rho_n$. As mentioned above Eq. (8), we assume the dependence of f_{bulk} on $\nabla \rho_n$ to be through a quadratic form, whose coefficients may depend on T and ρ_n . Below, as in Appendix A of Ref. [20], we consider a quasistatic deformation of a mixture to derive Eqs. (9) and (10). We write V_t for a small region co-moving with the deformation. Here, t is not time but a parameter of the deformation. In general, an infinitesimal change in the entropy are contributed independently from the mechanical work, from the change in the composition, and from the change in the internal energy. Thus, regarding T , Π , and μ_n as homogeneous over a small region V_t , we have

$$T \frac{d}{dt} \int_{V_t} d\mathbf{r} \tilde{s} = \Pi : \int_{\partial V_t} dA \mathbf{n}_{\partial V_t} \mathbf{v} - \mu_n \frac{d}{dt} \int_{V_t} d\mathbf{r} \rho_n(\mathbf{r}, t) + \frac{d}{dt} \int_{V_t} d\mathbf{r} u. \quad (\text{A3})$$

Here, the symbol $:$ is defined so that $\mathbf{A} : \mathbf{B} = A_{ij} B_{ji}$ holds for two tensors \mathbf{A} and \mathbf{B} , and $\mathbf{n}_{\partial V_t}$ is the outward facing unit normal vector of the surface of V_t .

Each locus of a mixture is assumed to have each bath of particles and heat. We here write \mathbf{j}_n and \mathbf{j}_u for their respective fluxes to the bath, and write \mathbf{v} for a displacement vector per unit value of t . The meanings of \mathbf{j}_n and \mathbf{v} are different from the ones in the text, respectively; $\mathbf{j}_a + \mathbf{j}_b$ does not always vanish here. Although t is not the time, we can treat t as the

time formally to define the Eulerian time-derivative $\partial/(\partial t)$ and Lagrangian time-derivative $D/(Dt)$. We have

$$\frac{D\rho_n}{Dt} = -\rho_n \nabla \cdot \mathbf{v} - \nabla \cdot \mathbf{j}_n \quad \text{and} \quad \frac{Du}{Dt} = -u \nabla \cdot \mathbf{v} - \nabla \cdot \mathbf{j}_u. \quad (\text{A4})$$

The whole region occupied by the mixture, V_{tot} , is deformable here, unlike in the text. The LHS of Eq. (A3) is rewritten as the integral of $T[D\tilde{s}/(Dt) + \tilde{s}\nabla \cdot \mathbf{v}]$ over V_t . Rewriting the last two terms on the RHS similarly and applying the divergence theorem for the first term, we obtain an equation for the integrands owing to arbitrariness of V_t . With the aid of this equation, the change in the entropy in V_{tot} per unit value of t is found to be

$$\int_{V_{\text{tot}}} d\mathbf{r} \left[\frac{D\tilde{s}}{Dt} + \tilde{s}\nabla \cdot \mathbf{v} \right] = \int_{V_{\text{tot}}} d\mathbf{r} \left[\frac{\Pi}{T} : \nabla \mathbf{v} + \frac{\mu_n}{T} \nabla \cdot \mathbf{j}_n - \frac{1}{T} \nabla \cdot \mathbf{j}_u \right], \quad (\text{A5})$$

where T , Π , and μ_n can be inhomogeneous. The factor $\nabla \cdot \mathbf{v}$ in Eqs. (A4) and (A5) comes from the change rate of the Jacobian between the Eulerian and Lagrangian coordinates. We have

$$\frac{D\tilde{s}}{Dt} = \frac{\partial \tilde{s}}{\partial u} \frac{Du}{Dt} + \frac{\partial \tilde{s}}{\partial \rho_n} \frac{D\rho_n}{Dt} + \frac{\partial \tilde{s}}{\partial (\nabla \rho_n)} \cdot \nabla \left(\frac{D\rho_n}{Dt} \right) - \frac{\partial \tilde{s}}{\partial (\nabla \rho_n)} \cdot (\nabla \mathbf{v}) \cdot (\nabla \rho_n), \quad (\text{A6})$$

which can be rewritten using Eqs. (A2) and (A4). Substituting the result into the LHS of Eq. (A5) and applying integration by parts, we find the LHS to be the sum of

$$- \int_{\partial V_{\text{tot}}} d\mathbf{r} \frac{1}{T} \frac{D\rho_n}{Dt} \frac{\partial f_{\text{bulk}}}{\partial (\nabla \rho_n)} \cdot \mathbf{n}_{\partial V_{\text{tot}}} \quad (\text{A7})$$

and the RHS of Eq. (A5) with μ_n and Π being replaced by the RHS's of Eqs. (9) and (10), respectively. This means that μ_n and Π are given by these equations, respectively. Because Π is symmetric, we can derive Eq. (12), or equivalently, $\nabla \cdot (\Pi/T) = \rho_n \nabla (\mu_n/T) - u \nabla (1/T)$, which is of the same form as Eq. (2.44) of Ref. [37]. Equation (9) can be used in calculating not only $\varphi^{(0)}$ but also $\varphi^{(1)}$; the latter need not be obtained in the present study.

We next consider thermodynamics of the mixture in a thin interfacial region regarded as ∂V_{tot} . The free energy per unit area of this region is denoted by f_{surf} in Eq. (8), and is here denoted by $f^{(s)}$. The superscript (s) in general indicates a thermodynamic quantity in ∂V_{tot} ; a density with the superscript represents a quantity per unit area. As in Eq. (20), we can introduce internal energy $u^{(s)}$ and entropy $s^{(s)}$ from $f^{(s)}$. These three quantities are functions of $T^{(s)}$ and $\rho_n^{(s)}$. As Eq. (A3) yields Eq. (A5), an equation for a

small co-moving area on ∂V_{tot} yields an equation representing the change of the entropy on ∂V_{tot} . Two points are to be noted in this derivation. First, the mechanical contribution consists of a term involving the two-dimensional pressure tensor $\Pi^{(s)}$ and a term involving the force normal to the small area. Because $f^{(s)}$ includes no gradients of mass densities, the pressure tensor is written as the two-dimensional scalar pressure multiplied by the identity tensor on ∂V_{tot} . The scalar pressure denoted by $P^{(s)}$. We define $P_n^{(s)}$ so that the normal force is $P_n^{(s)} \mathbf{n}_{\partial V_{\text{tot}}}$ per unit area. Second, the factor coming from the change rate of the Jacobian is not $\nabla \cdot \mathbf{v}$, appearing Eqs. (A4) and (A5), but $\nabla_{\parallel} \cdot \mathbf{v}_{\parallel} - 2H_m \mathbf{v} \cdot \mathbf{n}_{\partial V_{\text{tot}}}$, where \mathbf{v}_{\parallel} is the projection of \mathbf{v} on the plane tangential to ∂V_{tot} , $\nabla_{\parallel} \cdot \mathbf{v}_{\parallel}$ indicates the divergence defined on ∂V_{tot} , and H_m denotes the mean curvature of ∂V_{tot} [75]. The curvature is defined so that it is positive when the center of curvature lies on the side directed by $\mathbf{n}_{\partial V_{\text{tot}}}$.

The temperature at a local area on ∂V_{tot} , $T^{(s)}$, should be equal to T at its adjacent local region of V_{tot} . Similarly, $\rho_{\alpha}^{(s)}$ is determined by ρ_{α} at the adjacent region so that the former equals the latter multiplied by the interfacial region's width. No other factor is involved in determining $\rho_{\alpha}^{(s)}$, which means $\mu_{\alpha}^{(s)} = 0$. Through these relationships, $f_{\text{surf}}(T, \rho_n)$ equals $f^{(s)}(T^{(s)}, \rho_n^{(s)})$. Taking Eq. (A7) into account, we find

$$0 = \frac{\partial f_{\text{surf}}}{\partial \rho_n} + \frac{\partial f_{\text{bulk}}}{\partial (\nabla \rho_n)} \cdot \mathbf{n}_{\partial V} \quad \text{at} \quad \partial V \quad (\text{A8})$$

from the equation representing the change of the entropy on ∂V_{tot} . We also find $P^{(s)} = -f_{\text{surf}}$, which gives the Laplace pressure $P_n^{(s)} = -2f_{\text{surf}}H_m$ [76]. Notably, f_{surf} equals the grand-potential density of ∂V_{tot} owing to $\mu_n^{(s)} = 0$. We need not consider these interfacial forces and the force exerted on the mixture by the tube's wall in calculating the velocity field in the tube because the latter force is determined so that the no-slip condition is realized.

Appendix B: Reciprocal relations

We consider two sets of flow fields, each being driven by the thermodynamic forces $(-\delta(P/T)_k, -\delta(\mu_-/T)_k, \delta(1/T)_k)$, with k being i or ii. The resultant thermodynamic fluxes and fields in the tube are also indicated by the subscript k . Different ways of applying the divergence theorem to the volume integral of $\eta_s^{(0)} E_i^{(1)} : E_{ii}^{(1)}$ over the tube interior, denoted

by V_{tube} , give

$$\int_{V_{\text{tube}}} d\mathbf{r} \mathbf{v}_{\text{ii}}^{(1)} \cdot [\nabla \cdot (\eta_s^{(0)} E_i^{(1)})] = \int_{V_{\text{tube}}} d\mathbf{r} \mathbf{v}_i^{(1)} \cdot [\nabla \cdot (\eta_s^{(0)} E_{\text{ii}}^{(1)})] \quad (\text{B1})$$

with the aid of Eq. (16) and the no-slip condition at the tube's wall. Here, we neglect effects of tube's edges on the laminar flow. Substituting Eq. (28) into Eq. (B1), we find that

$$\int_{S_{\text{tube}}} dA v_{\text{ii},z}^{(1)} \left[\frac{\rho^{(0)}}{\rho^{(\text{ref})}} \delta \left(\frac{P}{T} \right)_i + \left(\varphi^{(0)} - \frac{\varphi^{(\text{ref})}}{\rho^{(\text{ref})}} \right) \delta \left(\frac{\mu_-}{T} \right)_i - \left(P^{(0)} + e^{(0)} - \frac{\rho^{(0)} e^{(\text{ref})}}{\rho^{(\text{ref})}} \right) \delta \left(\frac{1}{T} \right)_i \right] \quad (\text{B2})$$

equals the above equation with the subscripts i and ii exchanged. Putting $\delta(P/T)_i$, $\delta(\mu_-/T)_i$, $\delta(P/T)_{\text{ii}}$, and $\delta(1/T)_{\text{ii}}$ equal to zero, we use Eqs. (29), (30), (31), and (32) to find $L_{23} = L_{32}$. Likewise, we can obtain $L_{13} = L_{31}$ by putting $\delta(P/T)_i$, $\delta(\mu_-/T)_i$, $\delta(\mu_-/T)_{\text{ii}}$, and $\delta(1/T)_{\text{ii}}$ equal to zero. The other reciprocal relations can be derived similarly, as shown in Appendix B of Ref. [20].

Appendix C: Dissipative fluxes

In an equilibrium mixture, we consider a region where the mass densities are homogeneous. There, f_{bulk} is a function of T , ρ , and φ , and we have

$$\left(\frac{\partial \mu_-}{\partial \varphi} \right)_{T,P} = \left(\frac{\partial \mu_-}{\partial \varphi} \right)_{T,\rho} + \left(\frac{\partial \mu_-}{\partial \rho} \right)_{T,\varphi} \left(\frac{\partial \rho}{\partial \varphi} \right)_{T,P}. \quad (\text{C1})$$

The first partial derivative of the second term on the RHS above equals $\partial^2 f_{\text{bulk}} / (\partial \rho \partial \varphi)$, which vanishes because Eq. (48) is assumed. The second derivative does not diverge, as mentioned in Appendix D. Thus, whether T and P are fixed or T and ρ fixed, $\partial \mu_- / (\partial \varphi)$ are the same and are regarded as equal to the inverse of χ , which appears in Eq. (33). We have

$$\frac{1}{\chi} = \left(\frac{\partial \mu_-}{\partial c_a} \right)_{T,P} \left(\frac{\partial c_a}{\partial \varphi} \right)_{T,P} = \frac{1}{2\rho^2 \bar{v}_+} \left(\frac{\partial \mu}{\partial c_a} \right)_{T,P}, \quad (\text{C2})$$

where \bar{v}_+ denotes $(\bar{v}_a + \bar{v}_b)/2$. The second equality above comes from Eq. (34) of Ref. [20]. Because a mixture we consider has $\rho \bar{v}_+ \approx 1$ [20], Eq. (33) is consistent with the result in Refs. [46, 77].

With $\bar{\delta}$ indicating the deviation from the average, the thermodynamic forces are $\bar{\delta}(1/T)$, $-\bar{\delta}(\mu_+/T)$, and $-\bar{\delta}(\mu_-/T)$ in Eq. (22). This equation is rewritten as

$$\mathbf{j} = -4\tilde{\alpha}\nabla\mu_- + 2\tilde{\beta}\nabla T \quad \text{and} \quad \mathbf{j}_q - \mu_- \mathbf{j} = 2T\tilde{\beta}\nabla\mu_- - \tilde{\gamma}\nabla T, \quad (\text{C3})$$

whereby $\tilde{\alpha}$, $\tilde{\beta}$, and $\tilde{\gamma}$ are defined. We write $\check{s}(\equiv s/\rho)$ for entropy per unit mass. As can be seen from Ref. [78], the irreversible fluxes of c_a and \check{s} are respectively given by the quotient of the first entry in Eq. (C3) divided by 2ρ and that of the second divided by ρT , whereas the conjugate thermodynamic forces are respectively given by $-2\rho(\bar{\delta}\mu_-)/T$ and $-\rho(\bar{\delta}T)/T$. After the division, the second term on the RHS of the second entry becomes equal to the product of $-\rho(\nabla T)/T$ multiplied by $\tilde{\gamma}/\rho^2$, which is one of the Onsager coefficients. Similarly, we can obtain the other Onsager coefficients. Comparing Eq. (22) with (C3), we obtain

$$\Lambda = 4\tilde{\alpha}, \quad \kappa = 2T \left(2\mu_- \tilde{\alpha} - T\tilde{\beta} \right), \quad \text{and} \quad \lambda = 4\mu_- T \left(\mu_- \tilde{\alpha} - T\tilde{\beta} \right) + T^2 \tilde{\gamma}. \quad (\text{C4})$$

In Refs. [46, 77, 79], the singular parts of the LHS's above, indicated by the subscript sing , are shown to satisfy

$$\frac{\tilde{\beta}_{\text{sing}}}{2\tilde{\alpha}_{\text{sing}}} = - \left(\frac{\partial c_a}{\partial T} \right)_{P, \mu_-} \left(\frac{\partial \mu_-}{\partial c_a} \right)_{T, P} = -\bar{s}_-, \quad (\text{C5})$$

whose second equality comes from Eq. (4), and

$$\frac{\tilde{\gamma}_{\text{sing}}}{4\tilde{\alpha}_{\text{sing}}} = \frac{\rho T}{\chi} \left(\frac{\partial \check{s}}{\partial T} \right)_{P, \mu_-} \approx T\bar{s}_-^2. \quad (\text{C6})$$

The approximate equality of Eq. (C6) is explained in the next paragraph. The background parts of $\tilde{\alpha}$ and $\tilde{\beta}$ are negligible in the critical regime [45, 57, 73, 80]. Because of the singular properties, the Ludwig-Soret effect has universal properties in a near-critical binary fluid mixture [46, 77, 80–82]. For $\tilde{\gamma}$, neglecting the background part and adopting the approximate equality, we obtain Eq. (35), which leads to neglect of the thermal conductivity not exhibiting the critical enhancement [77].

The partial derivative in Eq. (C6) equals

$$\left(\frac{\partial \check{s}}{\partial T} \right)_{P, c_a} + \left(\frac{\partial \check{s}}{\partial c_a} \right)_{T, P} \left(\frac{\partial c_a}{\partial T} \right)_{P, \mu_-} = \frac{c_P}{\rho T} + 2\bar{s}_- \left(\frac{\partial c_a}{\partial T} \right)_{P, \mu_-}, \quad (\text{C7})$$

where c_P denotes the isobaric specific heat under constant c_a . The equality between the second terms on both sides above comes from a Maxwell relation and Eq. (4). The second

partial derivative in Eq. (C5) can be rewritten using Eq. (34) of Ref. [20]. As a result, the last partial derivative in Eq. (C7) equals $\bar{s}_-\chi/(2\rho^2\bar{v}_+)$. As mentioned in Appendix D, c_P diverges more weakly than χ in the critical regime, where the approximate equality in Eq. (C6) is valid. Without the above-mentioned approximations for $\tilde{\gamma}$, the area integral of T^2 multiplied by the sum of the thermal conductivity and $\Lambda c_P/\chi$, evaluated at $\varepsilon = 0$, over S_{tube} should be added to the RHS of Eq. (45).

An alternative explanation is as follows. In the mode-coupling theory, the singular part of an Onsager coefficient is calculated in terms of the time-integral of the two-time correlation function of the reversible fluxes, as mentioned in Section 6.5 of Ref. [31]. The Onsager coefficients mentioned above Eq. (C4) are found to be $\tilde{\gamma}/\rho^2$, $-\tilde{\beta}T/\rho^2$, and $\tilde{\alpha}T/\rho^2$, and their singular parts are linked with the autocorrelation of $(\bar{\delta}\tilde{s})\mathbf{v}$, the crosscorrelation of $(\bar{\delta}\tilde{s})\mathbf{v}$ and $(\bar{\delta}c_a)\mathbf{v}$, and the autocorrelation of $(\bar{\delta}c_a)\mathbf{v}$, respectively. This means that, in the critical regime, the ratio of $\tilde{\gamma}_{\text{sing}}$ to $-\tilde{\beta}_{\text{sing}}T$ and that of $-\tilde{\beta}_{\text{sing}}T$ to $\tilde{\alpha}_{\text{sing}}T$ are given by $\partial\tilde{s}/(\partial c_a)$ with T and P fixed, which is consistent with Eqs. (C5) and (C6).

Appendix D: Internal-energy fluctuations and approximate incompressibility

Here, we discuss some backgrounds of Eq. (48). In the bare model, without the contribution from ∂V_{tot} taken into account, we define the effective Hamiltonian \mathcal{H} so that the equilibrium probability density functional (EPDF) of ρ and ψ is proportional to $e^{-\mathcal{H}}$. As mentioned in the text, \mathcal{H} includes the ψ^4 model,

$$\int_{V_{\text{tot}}} d\mathbf{r} \left[\frac{1}{2}A_0\tau\psi^2 + \frac{\lambda_0}{4!}\psi^4 + \frac{a_0^2}{2}|\nabla\psi|^2 \right], \quad (\text{D1})$$

where $\lambda_0(> 0)$ and a_0 are constants, and the integrand above becomes a part of Eq. (48) divided by $k_B T$ after coarse-grained. The value of T_c in the definition of τ depends on the stage of the coarse-graining. Writing m for $(u - u_c)/(k_B T_c)$, we can also consider the EPDF of ρ , ψ , and m . We define \mathcal{H}_s so that this EPDF is proportional to $e^{-\mathcal{H}_s}$ in the bare model. Integrating out m from this EPDF should yield the EPDF of ρ and ψ . In other words, the latter's Legendre transform is the former, and vice versa. Thus, owing to a term $A_0\tau\psi^2/2$ in \mathcal{H} , \mathcal{H}_s has a term proportional to $m\psi^2$ and \mathcal{H} has a term proportional to τ^2 [31, 51]. We define C_0 so that this term equals $-C_0\tau^2/(2k_B)$, and the variance of m is proportional to

C_0 . Coarse-graining the ψ^4 model and imposing the self-consistent condition for off-critical compositions set up the RLFT [39]. We can also set it up by coarse-graining \mathcal{H}_s , imposing a self-consistent condition, and integrating out m . In this procedure, C_0 becomes C of Eq. (48) because fluctuations of m are affected by those of ψ via their coupling term [31, 51]. Instead of using Eq. (48) as it is, we can calculate $\hat{\sigma}^{(\text{th})}$ by evaluating the dependence of C on ξ locally. Although data are not shown, the resultant changes from the results of Fig. 3 are negligibly small.

The isochoric specific heat c_V , given by $-T\partial^2 f_{\text{bulk}}/(\partial T^2)$ with ρ and φ being fixed, remains finite at the critical point, although it appears to diverge in the regime accessible to usual experiments [31, 83]. Linked with the fluctuations of m , the isobaric specific heat c_P becomes proportional to C ($\propto |\tau|^{-\alpha}$ with $\alpha = 0.11$) in the critical regime with c_a being the value at the critical point [31, 84]. The same power-law dependence is shared by the isothermal compressibility κ_T and the thermal expansion coefficient α_P , which are given by

$$\kappa_T = \left. \frac{1}{\rho} \frac{\partial \rho}{\partial P} \right)_{T, c_a} \quad \text{and} \quad \alpha_P = - \left. \frac{1}{\rho} \frac{\partial \rho}{\partial T} \right)_{P, c_a} = \kappa_T \left. \frac{\partial P}{\partial T} \right)_{\rho, c_a}. \quad (\text{D2})$$

These quantities are related with each other via $\kappa_T (c_P - c_V) = \alpha_P^2 T$. The singularity of κ_T is generated by coupling between $\rho - \rho_c$ and ψ^2 in the ρ -dependent part in the EDPF. We neglect this coupling in Eq. (48), considering that the singularity is not accessible to usual experiments [31, 85]. Observed values of κ_T and α_P are typically 10^{-9} Pa^{-1} and 10^{-3} K^{-1} , respectively, near the critical point [85, 86].

In this paragraph, we show that the last partial derivative of Eq. (C1) is finite. In the region mentioned at the beginning of Appendix C, we simply write f for f_{bulk} and refer to its derivatives by adding subscripts. For example, $f_{\rho\varphi}$ represents $\partial^2 f_{\text{bulk}}/(\partial\rho\partial\varphi)$, which vanishes because Eq. (48) is assumed. We have

$$\delta P = \rho (f_{\rho\rho}\delta\rho + f_{\rho T}\delta T) + \varphi (f_{\varphi\varphi}\delta\varphi + f_{\varphi T}\delta T) + s\delta T \quad (\text{D3})$$

owing to Eq. (7). Here, unlike in the text, δ indicates an infinitesimal change. Using Eq. (D3) and $\varphi = \rho(2c_a - 1)$, we find $\delta\varphi$ ($\delta\rho$) equal to φ (ρ) multiplied by

$$\delta P \frac{1}{\rho^2 f_{\rho\rho} + \varphi^2 f_{\varphi\varphi}} \quad (\text{D4})$$

when T and c_a are fixed. The fraction is found to equal κ_T because of the first entry of Eq. (D2) and Eq. (D3). Considering that the sum in the first (second) parentheses of Eq. (D3) equals $\delta\mu_+$ ($\delta\mu_-$), we use Eq. (D4) to find that the first entries of Eqs. (4) and (5) give $\bar{v}_- = \varphi f_{\varphi\varphi} \kappa_T$ and $\bar{v}_+ = \rho f_{\rho\rho} \kappa_T$. Thus, we use Eq. (D3) to find that the last partial derivative in Eq. (C1) equals $-\bar{v}_-/\bar{v}_+$, which result holds if $f_{\rho\varphi}$ does not vanish. The limit of this fraction obtained as the critical point is approached can be written in terms of ρ_c and φ_c and is finite, which supports the description below Eq. (C1).

Finally, we consider validity of $\rho^{(\text{ref})} \approx \rho_c$; $\rho^{(\text{ref})}$ appears in Eq. (61) and is involved in returning the dimension to $\hat{G}^{(\text{th})}$. For definiteness, we here write $\tau^{(\text{ref})}$ for the value of τ in the reference state. At the state we reach by changing τ from zero to $\tau^{(\text{ref})}$ with P and c_a being fixed, how ρ changes from ρ_c can be approximately calculated from the regular part of α_P [85]. The difference between the value of ρ at this state and $\rho^{(\text{ref})}$ can be calculated using the last partial derivative in Eq. (C1). Thus, we can calculate the difference $\rho^{(\text{ref})} - \rho_c$, and find that the difference divided by ρ_c is smaller than 10^{-3} for $\tau^{(\text{ref})} = 1/300$ in magnitude. Thus, we can use $\rho^{(\text{ref})} \approx \rho_c$.

Appendix E: Approximation in the derivation of Eq. (56)

By using Eq. (D3) to calculate the second entry of Eq. (4), we obtain $\bar{s}_- = \varphi f_{\varphi\varphi} \alpha_P - f_{\varphi T}$. The term $\mu_-^{(\text{ref})} \varphi$ is included in f_- , as shown in Eq. (51). Its contribution to the second entry of Eq. (20) is

$$-T^2 \frac{\partial}{\partial T} \Bigg|_{\rho, \varphi} \frac{\mu_-^{(\text{ref})} \varphi}{T} = \mu_-^{(\text{ref})} \varphi - T \varphi \frac{\partial}{\partial T} \Bigg|_{\rho, \varphi} \mu_-^{(\text{ref})}. \quad (\text{E1})$$

The value of the last partial derivative above equals that of $f_{\varphi T}$ in the reference state owing to $f_{\rho\varphi} = 0$. Thus, because of Eq. (34), Eq. (E1) consists of $\bar{H}_-^{(\text{ref})} \varphi$ and the other term. This term gives an extra term

$$\frac{T_* \tau_*}{\mu_*} (\varphi f_{\varphi\varphi} \alpha_P)^{(\text{ref})} \hat{\psi}^{(0)} \quad (\text{E2})$$

to Eq. (59), where the superscript (ref) implies that the product in the parentheses should be evaluated in the reference state. We can use Eq. (63) to evaluate $f_{\varphi\varphi}$ and find Eq. (E2) to be smaller than $30|\tau|^\gamma |\hat{\psi}^{(0)}|$ in magnitude. This magnitude is found to be much smaller than the corresponding magnitude given by the circles in Fig. 3, with the aid of values of

$\hat{\psi}^{(0)}$ in Fig. 2. Thus, Eq. (E2) is negligible in deriving Eq. (56).

Appendix F: Thermoosmotic flow far from a flat surface

For a mixture occupying a semi-infinite space bounded by a flat wall surface, we consider imposing a temperature gradient along the z axis, which is parallel to the wall surface. The equilibrium profile $\psi^{(0)}$ is regarded as a function of the distance from the surface, denoted by X , and is assumed to approach zero as $X \rightarrow \infty$. The velocity field can be calculated similarly to Eq. (60). Assuming that η_s to be η_* homogeneously and using Eq. (71), we find that the z component of the mixture velocity far from the surface, or the slip velocity, is approximately given by

$$\frac{k_B C_1 |\tau|}{2\eta_* \xi_0^2 \tau} \int_0^X dX_1 \int_{X_1}^\infty dX \omega^{\gamma-1} [\psi^{(0)}(X)]^2 \quad (\text{F1})$$

multiplied by the z component of the temperature gradient.

When the second term is much smaller than the first term on the RHS of Eq. (52), $\hat{\omega} \approx |\hat{\tau}|$ holds and the second term on the RHS of Eq. (50) is negligible. We further approximate M_- to be $k_B T_c C_1$ to obtain the free-energy density in the Gaussian model, where ξ becomes homogeneous and $\psi^{(0)}(X)$ equals $h\xi e^{-X/\xi}/M_-$ [87, 88]. Substituting this into Eq. (F1) with $\omega = |\tau|$ and $h = 0.1 \text{ cm}^3/\text{s}^2$, we find that the slip velocity in terms of $\hat{v}_z^{(\text{th})}$ for a mixture of LW (NEMP) is -0.082 (0.12) at $|\tau| = 3.2 \times 10^{-3}$, and -0.017 (0.025) at $|\tau| = 6.4 \times 10^{-3}$. Here, for the critical exponents, we use the values mentioned in Section III C, not the values in the Gaussian model. These values of the slip velocity are comparable with the corresponding values calculated in the same procedure as used for Fig. 5, which are -0.042 (0.061) at $|\tau| = 3.2 \times 10^{-3}$ and -0.014 (0.021) at $|\tau| = 6.4 \times 10^{-3}$.

The equilibrium profile $\psi^{(0)}(X)$ becomes universal in the adsorption layer as the critical point is approached beyond the regime of the Gaussian model [25, 33, 34]. As is done for the diffusioosmosis in Appendix D of Ref. [20] and in Section VC of Ref. [36], we use the universal profile $\psi^{(0)}(X) \propto X^{-\beta/\nu}$ in Eq. (F1). With the aid of Eq. (52), we find that the slip velocity in thermoosmosis becomes proportional to $|\tau|^{\nu-1}$ as τ approaches zero.

-
- [1] A. P. Bregulla, A. Würger, K. Günther, M. Mertig, and F. Cichos, “Thermo-osmotic flow in thin films,” *Phys. Rev. Lett.* **116**, 188303 (2016).
- [2] C. Lee, C. Cottin-Bizonne, A.-L. Biance, P. Joseph, L. Bocquet, and C. Ybert, “Osmotic flow through fully permeable nanochannels,” *Phys. Rev. Lett.* **112**, 244501 (2014).
- [3] S. Shin, “Diffusiophoretic separation of colloids in microfluidic flows,” *Phys. Fluids* **32**, 101302 (2020).
- [4] S. Shakib, B. Rogez, S. Khadir, J. Polleux, A. Würger, and G. Baffou, “Microscale thermophoresis in liquids induced by plasmonic heating and characterized by phase and fluorescence microscope,” *J. Phys. Chem. C* **125**, 21533–21542 (2021).
- [5] W. Q. Chen, M. Sedighi, and A. P. Jivkov, “Thermo-osmosis in hydrophilic nanochannels: mechanism and size effect,” *Nanoscale* **13**, 1696–1716 (2021).
- [6] R. Ganti, Y. Liu, and D. Frenkel, “Molecular simulation of thermo-osmotic slip,” *Phys. Rev. Lett.* **119** 038002 (2017).
- [7] R. Piazza and A. Parola, “Thermophoresis in colloidal suspensions,” *J. Phys.:Condens. Matter* **20**, 153102 (2008).
- [8] A. Würger, “Thermal non-equilibrium transport in colloids”, *Rep. Prog. Phys.* **73**, 126601 (2010).
- [9] S. Marbach and L. Bocquet, “Osmosis, from molecular insights to large-scale applications,” *Chem. Soc. Rev.* **48**, 3102-3144 (2019).
- [10] E. Mangaud and B. Rotenberg, “Sampling mobility profiles of confined fluids with equilibrium molecular dynamics simulations,” *J. Chem. Phys.* **153**, 044125 (2020).
- [11] S. Ramírez-Hinestrosa and D. Frenkel, “Challenges in modelling diffusiophoretic transport,” *Eur. Phys. J. B* **94**, 199 (2021).
- [12] B. V. Derjaguin, N. Churaev, and V. Muller, *Surface Forces* (Springer Science+Business Media, LLC, Berlin, 1987).
- [13] B. V. Derjaguin, “Some results from 50 years’ research on surface forces,” In *Surface Forces and Surfactant Systems, Progress in Colloid & Polymer Science 74* (Steinkopff, Dresden, 1987) 17–30.

- [14] J. L. Anderson, “Colloid transport by interfacial forces,” *Ann. Rev. Fluid Mech.* **21**, 61–99 (1989).
- [15] B. V. Derjaguin and G. P. Sidorenkov, “On thermo-osmosis of liquid in porous glass,” *CR Acad. Sci. URSS* **32**, 622–626 (1941).
- [16] B. V. Derjaguin, G. P. Sidorenkov, E. A. Zubashchenkov, and E. V. Kiseleva E V, “Kinetic phenomena in boundary films of liquids,” *Kolloidn. Zh.* **9**, 335–347 (1947).
- [17] B. V. Derjaguin, S. S. Dukhin, and M. M. Koptelova, “Capillary osmosis through porous partitions and properties of boundary layers of solutions,” *J. Colloid. Interface Sci.* **38**, 584–595 (1972).
- [18] L. Fu, S. Merabia, and L. Joly, “What controls thermo-osmosis? Molecular simulations show the critical role of interfacial hydrodynamics,” *Phys. Rev. Lett.* **119**, 214501 (2017).
- [19] P. Anzini, G. M. Colombo, Z. Filiberti, A. Parola, “Thermal forces from a microscopic perspective,” *Phys. Rev. Lett.* **123**, 028002 (2019).
- [20] S. Yabunaka and Y. Fujitani, “Isothermal transport of a near-critical binary fluid mixture through a capillary tube with the preferential adsorption,” *Phys. Fluids* **34**, 052012 (2022).
- [21] D. Beysens and S. Leibler, ”Observation of an anomalous adsorption in a critical binary mixture,” *J. Physique Lett.* **43**, 133–136 (1982).
- [22] M. Schlossman, X-L. Wu, and C. Franck, “Order-parameter profile at long distances in an adsorbed binary liquid mixture near criticality,” *Phys. Rev. B* **31**, 1478–1485 (1985).
- [23] M. N. Binder, *Phase Transitions and Critical Phenomena VIII*, Critical behavior at surfaces. (Academic, London, 1983).
- [24] H. W. Diehl, *Phase Transition and Critical Phenomena X*, Field theoretical approach to critical behavior at surfaces. (Academic, London, 1986).
- [25] H. W. Diehl, ”The theory of boundary critical phenomena,” *Int. J. Mod. Phys. B* **11**, 3503–3523 (1997).
- [26] B. M. Law, “Wetting, adsorption, and surface critical phenomena,” *Prog. Surf. Sci.* **66**, 159–216 (2001).
- [27] S. Yabunaka and Y. Fujitani, “Drag coefficient of a rigid spherical particle in a near-critical binary fluid mixture, beyond the regime of the Gaussian model,” *J. Fluid Mech.* **886** A2 (2020).
- [28] K. Kawasaki, “Kinetic equations and time correlation functions of critical fluctuations,”

- Ann. Phys. (N.Y.) **61**, 1 (1970)
- [29] J. V. Sengers, “Transport properties near critical points,” *Int. J. Thermophys.* **6**, 203–232 (1985).
- [30] E. D. Siggia, P. C. Hohenberg, and B. I. Halperin, “Renormalization-group treatment of the critical dynamics of the binary-fluid and gas-liquid transitions,” *Phys. Rev. B* **13**, 2110–2123 (1976).
- [31] A. Onuki, *Phase Transition Dynamics* (Cambridge University Press, Cambridge, 2002), Sections 2.3, 3.1, 4.3, and 6.5.
- [32] R. Folk and G. Moser, “Critical dynamics: a field-theoretical approach,” *J. Phys. A: Math. Gen.* **39**, R207–R313 (2006).
- [33] M. E. Fisher and P. G. de Gennes, “Phénomènes aux parois dans un mélange binaire critique,” *C. R. Acad. Sci. Paris B* **287**, 207 (1978).
- [34] J. Rudnick and D. Jasnow, “Order-parameter profile in semi-infinite systems at criticality,” *Phys. Rev. Lett.* **48**, 1059 (1982).
- [35] Y. Fujitani, “Diffusiophoresis in a near-critical binary fluid mixture,” *Phys. Fluids* **34**, 041701 (2022).
- [36] Y. Fujitani, “Effects of the preferential adsorption in a near-critical binary fluid mixture on dynamics of a droplet,” *Phys. Fluids* **34**, 092007 (2022).
- [37] A. Onuki, “Dynamic van der Waals theory,” *Phys. Rev. E* **75**, 036304 (2007).
- [38] G. Gonnella, A. Lamura, and A. Piscitelli, “Dynamics of binary fluid mixtures in inhomogeneous temperatures,” *J. Phys. A: Math. Theor.* **41** 105001 (2008).
- [39] R. Okamoto and A. Onuki, “Casimir amplitude and capillary condensation of near-critical binary fluids between parallel plates: renormalized local functional theory,” *J. Chem. Phys.* **136**, 114704 (2012).
- [40] S. Yabunaka and Y. Fujitani, “Universal direction in thermoosmosis of a near-critical binary fluid mixture,” submitted.
- [41] S. R. de Groot and G. Mazur, *Non-equilibrium thermodynamics*, (Dover, New York, 1984). Chapters XI and XV.
- [42] S. Kjelstrup, D. Bedeaux, E. Johannessen, and J. Gross, *Non-Equilibrium Thermodynamics for Engineers* (World Scientific, New Jersey, 2017).
- [43] B. I. Halperin, P. C. Hohenberg, and E. D. Siggia, “Renormalization-group calculations of

- divergent transport coefficients at critical point,” *Phys. Rev. Lett.* **32**, 1289 (1974).
- [44] T. Ohta, “Selfconsistent calculation of dynamic critical exponents for classical liquid,” *Prog. Theor. Phys.* **54**, 1566 (1975).
- [45] S. Z. Mirzaev, R. Behrends, T. Heimburg, J. Haller, and U. Kaatzke, “Critical behavior of 2,6-dimethylpyridine-water: Measurements of specific heat, dynamic light scattering, and shear viscosity,” *J. Chem. Phys.* **124** 144517 (2006).
- [46] L. Mistura, “Transport coefficients near a critical point in multicomponent fluid system,” *Nuovo Cimento B* **12**, 35–42.
- [47] J. S. Walker and C. A. Vause, “Reappearing phases,” *Sci. Am.* **256**, 98-100 (1987).
- [48] M. Toda, S. Kajimoto, S. Toyouchi, T. Kawakatsu, Y. Akama, M. Kotani, and H. Fukumura, “Phase behavior of a binary fluid mixture of quadrupolar molecules,” *Phys. Rev. E* **94**, 052601 (2016).
- [49] Z. Chernia and Y. Tsori, “Hydrogen bonding of dimethylpyridine clusters in water: correlation between the lower consolute solution temperature and electron interaction energy,” *J. Chem. Phys.* **152**, 204304 (2020).
- [50] A. Pelissetto and E. Vicari, “Critical phenomena and renormalization-group theory,” *Phys. Rep.* **368**, 549 (2002).
- [51] B. I. Halperin, P. C. Hohenberg, and S. Ma, “Renormalization-group methods for critical dynamics: I. recursion relations and effects of energy conservation,” *Phys. Rev. B* **10**, 139–153 (1973).
- [52] R. F. Berg and M. R. Moldover, “Critical exponent for the viscosity of four binary liquids,” *J. Chem. Phys.* **89**, 3694–3704 (1989).
- [53] R. F. Berg and M. R. Moldover, “Critical exponent for viscosity,” *Phys. Rev. A* **42**, 7183–7187 (1990).
- [54] T. A. Edison, M. A. Anisimov, and J. V. Sengers, “Critical scaling laws and an excess Gibbs energy model,” *Fluid Phase Equilibria* **150–151**, 429–438 (1998).
- [55] A. van’t Hof, M. Laura Japas, and C. J. Peters, “Description of liquid-liquid equilibria including the critical region with the crossover-NRTL model,” *Fluid Phase Equilibria* **192**, 27–48 (2001).
- [56] M. M. Olaya, P. Carbonell-Hermida, M. Trives, J. A. Labarta, and A. Marcilla, “Liquid-liquid equilibrium data correlation using NRTL model for different types of binary systems:

- upper critical solution temperature , lower critical solution temperature, and closed miscibility loops,” *Ind. Eng. Chem. Res.* **59**, 8469–8479 (2020).
- [57] I. Iwanowski, K. Leluk, M. Rudowski, and U. Kaatz, “Critical dynamics of the binary system nitroethane/3-methylpentane: Relaxation rate and scaling function,” *J. Phys. Chem. A* **110**, 4313–4319 (2006).
- [58] K. To, “Coexistence curve exponent of a binary mixture with a high molecular weight polymer,” *Phys. Rev. E.* **63**, 026108 (2001).
- [59] A. M. Wims, D. McIntyre, and F. Hynne, “Coexistence curve for 3-methylpentane-nitroethane near the critical point,” *J. Chem. Phys.* **50** 616 (1969).
- [60] J. K. Bhattacharjee, R. A. Ferrell, R. S. Basu, and J. V. Sengers, “Crossover function for the critical viscosity of a classical fluid,” *Phys. Rev. A*, **24**, 1469 (1981).
- [61] B. C. Tsai and D. McIntyre, ”Shear viscosity of nitroethane-3-methylpentane in the critical region,” *J. Chem. Phys.* **60**, 937 (1974).
- [62] A. Stein, S. J. Davidson, J. C. Allegra, and G. F. Allen, “Tracer Diffusion and Shear Viscosity for the System 2,6-Lutidine-Water near the Lower Critical Point,” *J. Chem. Phys.* **56** 6164 (1972).
- [63] C. A. Grattoni, R. A. Dawe, C. Y. Seah, and J. D. Gray, “Lower Critical Solution Coexistence Curve and Physical Properties (Density, Viscosity, Surface Tension, and Interfacial Tension) of 2,6-Lutidine + Water,” *Chem. Eng. Data*, **38**, 516–519 (1993).
- [64] H. M. Leister, J. C. Allegra, and G. F. Allen, “Tracer diffusion and shear viscosity in the liquid-liquid critical region,” *J. Chem. Phys.* **51** 3701 (1969).
- [65] D. Braun, and A. Libchaber, “Trapping of DNA by thermophoretic depletion and convection,” *Phys. Rev. Lett.* **89**, 188103 (2001).
- [66] H. Jiang, H. Wada, N. Yoshinaga, and M. Sano, “Manipulation of colloids by a nonequilibrium depletion force in a temperature gradient” , *Phys. Rev. Lett.* **102**, 208301 (2009).
- [67] Y. T. Maeda, A. Buguin, and A. Libchaber, “Thermal separation: interplay between the Soret effect and entropic force gradient,” *Phys. Rev. Lett.* **107**, 038301 (2011).
- [68] R. A. Omari, C. A. Grabowski, and A. Mukhopadhyay, “Effect of surface curvature on critical adsorption,” *Phys. Rev. Lett.* **103**, 225705 (2009).
- [69] D. Beysens, “Brownian motion in strongly fluctuating liquid,” *Thermodyn. Interfaces Fluid Mech.* **3**, 1—8 (2019).

- [70] F. J. Wegner, “Corrections to scaling laws,” *Phys. Rev. B* **5**, 4529–4536 (1972).
- [71] Z. Y. Chen, P. C. Albright, and J. V. Sengers, “Crossover from singular critical to regular classical thermodynamic behavior of fluids,” *Phys. Rev. A* **41**, 3161 (1990).
- [72] Z. Y. Chen, P. C. Albright, S. Tang, and J. V. Sengers, “Global thermodynamic behavior of fluids in the critical region,” *Phys. Rev. A* **42**, 4470 (1990).
- [73] R. Folk and G. Moser, “Critical dynamics in mixtures,” *Phys. Rev. E* **58**, 6246–6274 (1998).
- [74] De Gennes, P. G. and Prost, J. (1993). *The physics of liquid crystals* (Oxford Univ. Press, Oxford, 1993).
- [75] Y. Fujitani, “Dynamics of the lipid-bilayer membrane taking a vesicle shape,” *Physica A* **203**, 214–242 (1994). [Erratum: *ibid* **237**, (1997) 346–347].
- [76] Y. Fujitani, “Effective viscosity of a near-critical binary fluid mixture with colloidal particles dispersed dilutely under weak shear,” *J. Phys. Soc. Jpn.* **83**, 084401 (2014).
- [77] J. Luettmmer-Strathmann, “Thermal diffusion in the critical region,” In *Thermal nonequilibrium phenomena in Fluid Mixtures (Lecture Notes in Physics 584)* (Springer, Berlin, 2002), 24–37.
- [78] L. D. Landau and E. M. Lifshitz, *Fluid Mechanics, 2nd Ed.* (Elsevier, Amsterdam, 1987), §58.
- [79] M. A. Anisimov, A. V. Voronel, and E. E. Gorodetskii, “Isomorphism of critical phenomena,” *Sov. Phys. JETP* **33**, 605 (1971).
- [80] M. Giglio and A. Vendramini, “Thermal-diffusion measurements near a consolute critical point,” *Phys. Rev. Lett.* **34** 561–564 (1975).
- [81] I. I. Ryzhkov and S. V. Kozlova, “Stationary and transient Soret separation in a binary mixture with a consolute critical point,” *Eur. Phys. J. E* **39**, 130 (2016).
- [82] W. Köhler and K. I. Mozorov, “The Soret effect in liquid mixtures – a review,” *J. Non-Equilib. Thermodyn.* **41**, 151-197 (2016).
- [83] M. A. Anisimov, A. V. Voronel, and T. M. Ovodova, “The behavior of thermodynamical quantities near the critical line of an incompressible liquid mixture”, *Sov. Phys. JETP* **35**, 536–539 (1972).
- [84] M. A. Anisimov, E. E. Gorodetskii, V. D. Kulikov, A. A. Povodyrev, J. V. Sengers, “A general isomorphism approach to thermodynamic and transport properties of binary fluid mixtures near critical points,” *Physica A* **220**, 277–324 (1995).
- [85] E. A. Clerke and J. V. Sengers, “Fast pressure quenches near the critical point of a binary

- liquid mixture,” *Physica* **118A**, 360–370 (1983).
- [86] F. Pousaneh, O. Edholm, and A. Maciołek, “Molecular dynamics simulation of a binary mixture near the lower critical point,” *J. Chem. Phys.* **145**, 014501 (2016).
- [87] Y. Fujitani, “Undulation amplitude of a fluid membrane in a near-critical binary fluid mixture calculated beyond the Gaussian model supposing weak preferential attraction,” *J. Phys. Soc. Jpn.* **86**, 044602 (2017).
- [88] Y. Fujitani, “Relaxation rate of the shape fluctuation of a fluid membrane immersed in a near-critical binary fluid mixture,” *Eur. Phys. J. E* **39**, 31 (2016).